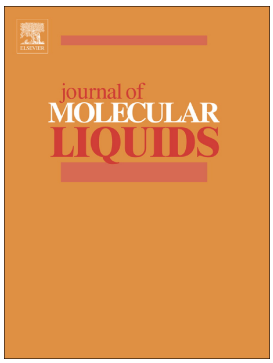

The unseen evidence of reduced Ionicity: The elephant in (the) room temperature ionic liquids

Alessandro Mariani, Matteo Bonomo, Xinpei Gao, Barbara Centrella, Alessandro Nucara, Roberto Buscaino, Alessandro Barge, Nadia Barbero, Lorenzo Gontrani, Stefano Passerini

PII: S0167-7322(20)37311-6

DOI: https://doi.org/10.1016/j.molliq.2020.115069

Reference: MOLLIQ 115069

To appear in: *Journal of Molecular Liquids*

Received date: 12 September 2020

Revised date: 26 November 2020

Accepted date: 11 December 2020

Please cite this article as: A. Mariani, M. Bonomo, X. Gao, et al., The unseen evidence of reduced Ionicity: The elephant in (the) room temperature ionic liquids, *Journal of Molecular Liquids* (2020), https://doi.org/10.1016/j.molliq.2020.115069

The unseen evidence of Reduced Ionicity: the elephant in (the) room temperature Ionic Liquids

Alessandro Mariani,*[a,b,c] Matteo Bonomo,[c,d] Xinpei Gao,[a,b] Barbara Centrella,[c,d] Alessandro Nucara,[e] Roberto Buscaino,[d] Alessandro Barge,[f] Nadia Barbero,[d] Lorenzo Gontrani,[c,g] and Stefano Passerini,*[a,b]

[a]Helmholtz Institute Ulm (HIU), Helmholtzstrasse 11, 89081 Ulm, Germany.

[b]Karlsruhe Institute of Technology (KIT), P.O. Box 3640, 76021 Karlsruhe, Germany.

[c]Department of Chemistry, Sapienza University of Rome, P. le Aldo Moro 5, 00185 Rome, Italy

[d]Department of Chemistry and NIS Interdepartmental Centre and INSTM Reference Centre, University of Turin, via Pietro Giuria 7, 10125 Turin, Italy

[e]Department of Physics, Sapienza University of Rome, P. le Aldo Moro,5 00185, Rome, Italy

[f] Department of Drug Science and Technology, University of Turin, via Pietro Giuria 7, 10125 Turin, Italy

[g]Department of Industrial Engineering, University of Rome, Tor Vergata, Viale degli Ingegneri, I-00133 Rome, Italy

Abstract

The unambiguous quantification of the proton transfer in Protic Ionic Liquids (PILs) and its differentiation from the concept of ionicity are still unsolved questions. Albeit researchers awfully quickly treat them as synonyms, the two concepts are intrinsically different and imply a dramatic modification in the expected chemical and physical properties of a PIL. Some attempts have been made to shed light on this discrimination, but single technique-based approaches fail in giving a clear answer. Aiming at definitively figuring out the differentiation between proton transfer and ionicity, we performed a multi-technique analysis (NMR, Raman, IR, thermal and electrochemical analyses, among others). Indeed, thermal and spectroscopic analyses are employed to determine the acid strength's role in ions' complete formation. To overcome the ambiguity between ionicity and formation degree, we introduce a new paradigm where Reduced Ionicity accounts for both the quantities mentioned above. The reduced ionicity directly affects the thermal stability, the phase behavior, and the spectroscopic observations, resulting in particular features in NMR and vibrational spectra. The combination of physical-chemical analyses and Pulsed-Gradient Spin-Echo (PGSE) NMR allows determining the reduced ionicity (and not the ionicity, as reported so far) of the investigated systems. In this context, being the proton transfer not quantitatively accessible directly, the reduced ionicity of a reference series of triethylamine-based PILs is investigated through transport properties as a function of temperature. Our findings point toward a substantial dependence of the reduced ionicity by the acid strength and the anion's coordination power. Furthermore, some interesting insights about the proton transfer are obtained, combining all the findings collected.

Introduction

Protic Ionic Liquids (PILs) are a sub-class of the nowadays widely studied ionic liquids[1–5] since they follow the general definition given by Walden in 1914, *i.e.*, "water-free salts that are in liquid form below 100 °C" [6]. A more rigorous definition is currently adopted as water-free organic salts showing a melting point at temperatures below their decomposition. Ionic liquids have been successfully applied in different fields ranging from sensors to solar cells and batteries, and they

can also be employed as lubricants in technological applications[7–15]. Indeed, interactions leading to PILs formation are constituted by a subtle balance of "weak" forces (*e.g.*, Coulombic interactions, hydrogen bonding, cohesion, and dispersion forces). ILs are generally classified into two prominent families: protic ionic liquids and aprotic ionic liquids (AILs). The former family results from the proton transfer between two neutral species[16], while the AILs are formed by the interaction of two preformed ions that, once mixed, give rise to the liquid system. As highlighted in Scheme 1, the reaction forming PILs is an equilibrium reaction, meaning that the parent compounds may always exist together with the ionic species. This apparent weakness in terms of stability of the ionic species can be turned into an advantage. While most AILs have almost zero vapor pressure, PILs precursors generally have low boiling points, enabling their distillation thanks to the Le Châtelier's principle[17]. Their ability to establish extended 3D hydrogen-bonded networks[18] gives rise to a series of exciting properties like enhanced proton mobility and peculiar solvation character as observed both experimentally[19–24] and by theoretical calculations[21,25,26]. PILs share morphologically similar hydrogen bond networks with water[27], although they differ in almost every aspect. The ease of preparation and the usually cheap precursors make them appealing materials for a wide range of applications[9]. Examples span from electrochemistry[28] to catalysis[29], the latter also thanks to their ability to dissolve a wide variety of compounds[30–35]. As PILs form via an equilibrium reaction, "neat" protic ionic liquids are not usually achieved, but some acid and base will be present in the system. To minimize the fraction of parent compounds, the use of strong acids and bases certainly helps. In this work, we employed triethylamine (TEA) as a Brønsted base in combination with a family of acids offering growing Brønsted acidity, *i.e.*, acetic acid (HAc), trifluoroacetic acid (HTFA), methanesulfonic acid (mesylic acid, HMs) and trifluoromethanesulfonic acid (triflic acid, HTfO), adhering to Scheme 1.

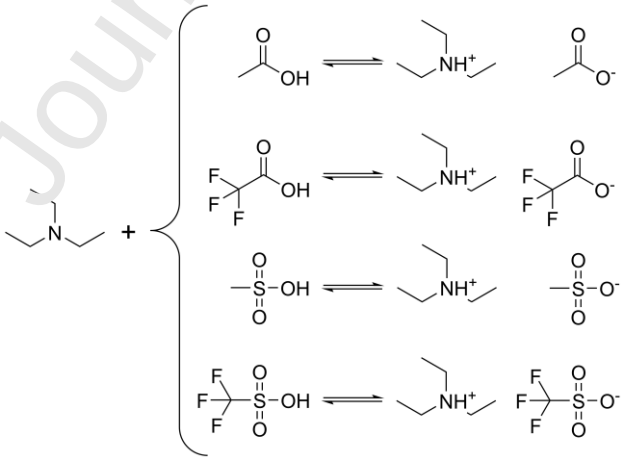

Scheme 1: Compounds discussed in this work. From top to bottom: Triethylammonium acetate; Tri-ethylammonium trifluoroacetate; Triethylammonium methanesulfonate; Triethylammonium trifluoro-methanesulfonate.

However, regarding triethylammonium acetate, a two-phase liquid was always obtained despite the synthetic route adopted, although previous reports indicated the successful synthesis of this compound[36–38]. In particular, we found the lower phase to be a mixture of the product and acetic acid in the mole ratio 1:3. Indeed, ^{1}H-NMR analyses (data

not shown) of the upper (colorless) and lower (brownish) phases suggest that the former, which has the smallest volume, is almost entirely made up of trimethylamine with the PIL present only in traces.

On the other hand, the lower and most abundant phase contains the final product and a significant excess of acetic acid. It should be noticed that the preparation protocol followed in the reports mentioned above [36–38] involved the distillation of the final product to remove the solvent. We may suggest that the amine-rich phase was lost upon distillation, resulting in the mixture of acetic acid and IL being misrecognized as a pure ionic liquid. In fact, in other manuscripts, the formation of two phases has been reported[39]. Recently, it was shown experimentally[40,41] and computationally[42] that the PIL is, indeed, not formed when equimolar quantities of triethylamine and acetic acid are mixed.

In the following, only the PILs resulting from the reaction of triethylamine (TEA) with either trifluoroacetic, mesylic, or triflic acid are considered because they form single-phase products. The determination of the proton transfer is often overlooked and sometimes confused with the ionicity of the system. The latter does not measure specifically the number of ionic species in the system, but it is instead a value indicating how many free charge carriers are present in the system. For an ionic liquid consisting of a cation A^+ and an anion B^-, the following expression defines the ionicity *I*:

$$I = \frac{[A^-] + [B^+]}{[A^-] + [B^+] + [A^-B^+]} \quad (1)$$

where the square brackets indicate the concentration of the species comprised, and $[A^-B^+]$ indicates the concentration of close ion-pairs. In order to be rigorous, the activity of the species should be used to calculate any thermodynamic quantity, but on first approximation, the use of concentrations could be accepted. It immediately appears clear how any neutral molecule is not included in the ionicity definition. In the case of protic ionic liquids, the cation carries a net charge due to protonation; thus, we will use HB^+ to indicate the cation. The subtle difference between the proton transfer and ionicity resides in the fact that the experimentally accessible quantities (*vide infra*) commonly used to determine ionicity can be decreased by three mostly independent factors: (i) the proton (back)transfer, (ii) the charge transfer between ions, and (iii) the ion association. Spectroscopic approaches have been proposed to quantify the proton transfer[43], but the method proposed relies on the assumption that the solvation shells and dielectric constant of the systems stay unperturbed upon changing the composition of the system, which is questionable. MacFarlane's group extensively addressed the proton transfer topic[39,44,45], but always accounting for ΔpK_a values, which are strictly meaningful only in aqueous systems. They also pointed to the proton transfer's qualitative spectroscopic determination [44], but again overlooking the different chemical environments experienced by the species in the Brønsted precursors and the ILs. Ionicity and proton transfer cannot be used as synonyms, albeit directly correlated[46]. The proton transfer (or Formation Degree, FD) is a thermodynamic quantity indicating the fraction of the Brønsted

precursors involved in the proton exchange reaction. For a Brønsted acid (HA) reaction with a Brønsted base (B) to form the PIL HB^+ A^-, we have:

$$K_{\mathrm{PT}} = \frac{[A^-] \cdot [HB^+]}{[HA] \cdot [B]} \quad (2)$$

$$\mathrm{FD} = \frac{[A^-] + [HB^+] + [A^-HB^+]}{[A^-] + [HB^+] + [A^-HB^+] + [HA] + [B]} \quad (3)$$

where K_{PT} is the equilibrium constant for the proton transfer.

The concept of charge transfer refers to the evidence of ions with non-integer electric charge[47–50]. Nevertheless, this effect, which is pivotal in aprotic ionic liquids[50,51], contributes only marginally to the ionicity value when Protic Ionic Liquids are considered. The charge transfer accounts for electron clouds sharing between ions (*i.e.,* negative charges moving from one species to another); on the other hand, proton transfer (*i.e.,* positive charges moving from one species to another) has a much more marked effect statistically and also in absolute value.

Strictly speaking, the concept of ionicity refers to the number of "free" ions in solution, as defined in Equation 1. Thus, the eventual formation of tight ion-pairs or the occurrence of other intermolecular interactions will not directly influence the proton transfer but will have a significant impact on system ionicity.

Triethylammonium triflate (TEATfO) and triethylammonium mesylate (TEAMS) have already been thoroughly investigated by Ludwig *et al.* [23,52–54]. However, they mainly focused on the spectroscopic characterization of these materials, simplistically assuming a complete formation of the PILs. Albeit they achieved a very in-depth knowledge of the systems, whether such systems are neat ILs or mixtures of ILs and their precursors is still undefined. Indeed, the second option seems to be the most likely. For example, Davidowsky *et al.*[55] investigated the ionicity of very similar systems (*i.e.*, TEA was replaced by diethyl-methyl amine, DEMA), finding an interesting correlation between the proton affinity of the acid in the gas phase and the PIL proton transfer: the lower the former, the higher the latter, resulting in the following order for the proton transfer: HAc < HTFA < HMS < HTfO. However, the ionicity of the DEMATfO was found to be as high as 0.61. We reasonably expect a higher ionicity in TEATfO, being TEA a stronger Brønsted base than DEMA. A remarkable effort in the proton transfer study in PILs has been made recently by Hasani *et al.* [56] employing ^{15}N NMR on a series of pyridine-based systems. They find a clear correlation between the difference of Brønsted precursors' proton affinities and the chemical shift of TEA nitrogen atom. Nevertheless, this approach does not return quantitative results, is limited to "ammonium" PILs, and requires ^{15}N labeled samples, which are substantially expensive.

Unfortunately, the proton transfer cannot be directly determined in practice. Many attempts have been made to employ potentiometric methods[57–61]. However, albeit the authors find reasonable correlations between proton transfer (*i.e.,* the number of neutral

species in the mixture) with the acid strength of the proton donor precursors, some points prevent us from relying on this approach entirely:
(i) no matter the IL investigated, two typical trends are evidenced: an almost quantitative proton transfer (related to a meager amount of neutral precursor) or an almost null proton transfer (IL not formed), whereas intermediate situations seem not to be detectable with this approach. (ii) The authors started from the assumption that a superacid (triflic acid, triflimidic acid (HTFSI)) in an aqueous environment could be used to titrate the unreacted base quantitatively. However, this assumption is not supported by experimental data regarding triflic acid strength in pure ionic liquids. For example, Kanzaki *et al.* [57,60] show how, in an IL, the H_3O^+ is a stronger acid than HNO_3, whereas the opposite is true in an aqueous environment. There is no evidence that HTfO or HTFSI are stronger acids than HNO_3 in the IL environment; thus, the proposed approach seems to be based on not universally valid assumptions. (iii) Moreover, the employment of triflic acid [60] or triflimidic acid [57] as a titration agent will lead to the formation of a ternary system in the investigated environment. Taking as example EAN, when triflic/triflimidic acid is added, the system becomes a mixture of EAN and EA-TfO/TFSI that could influence the linearity in the response of the electrochemical measurements. Finally, (iv) The reported approaches neglect the presence of water traces in the IL entirely. The latter's amount is calculated in the range of 50-100 ppm [57,60] for different ionic liquids corresponding to a mole percent in the range of 4-8% if we consider EAN. Practically speaking, the contribution of water should be considered at least when dealing with almost-completely-formed ILs: indeed, in these cases, the concentration of H_2O is higher than the one of the unreacted ethylamine, and its basicity could also be comparable if not higher (in IL environment) than the latter. If so, the titration would involve two different species (H_2O and Et-NH_2), and the quantification of the amine could be largely overestimated. The pioneering theoretical work of Ingenmey *et al.* [62] makes use of Quantum Cluster Equilibrium Theory to obtain several thermodynamic properties from two different PILs computationally. In that work, they find values for the proton activities in fair agreement with the ones determined with the potentiometric methods. On this basis, we aim to expand the current work by employing the experimental and computational techniques abovementioned in a forthcoming paper.
For now, we focused on measuring the systems' ionicity but considering the incomplete formation of the PILs while interpreting the results, *i.e.*, not only referring to ion association. In this work, we qualitatively prove that a certain degree of the examined PILs is always formed, no matter which acid is employed, through a spectroscopic approach. A first semi-quantitative analysis of the PILs ionicity is done by considering the so-called Walden plot, where the inverse of the viscosity is plotted against the molar conductivity[63]. Studies [46,64] proposed an empirical factor to derive the ionicity of a solution directly from the Walden plot: ΔW, the vertical distance from the bisector representing the ideal behavior, and the system's value. Angell's approach has been proven to be trustworthy for simple mixtures, but it mostly fails to predict the ionicity of more

complicated systems such as molten salts[65]. Concerning PILs, it could be considered a rule of thumb, whose validity should be further confirmed by additional evidence.

Finally, we employ Pulsed-Gradient Spin-Echo (PGSE) NMR as an elegant approach to measure self-diffusion coefficients (*D*) of the different species existing in a system[66,67]. This technique has been successfully employed in the study of pure ILs[68] and their mixtures with salts[69,70] and solvents[71,72]. Back in 2007, however, Annat *et al.*[73] proved that PGSE suffers from intrinsic internal gradients and can produce apparent diffusion coefficients considerably varying (up to 20%) for different protons within a given molecule. As a matter of fact, most common ILs are constituted by bulky ions. Thus, ^{1}H nuclei belonging to the same species may experience somewhat different environments. Therefore, the sizeable coupling will be present, and Brownian motion may not be sufficient to average out the dipolar interactions. Therefore, they resolved to PG stimulated echo (PGSTE) experiments, minimizing the issue. Currently, that method is the most exploited approach in the field of ILs[74]. In the present case, however, it should be pointed out that, since both the anion and the cation are relatively small, the classical PGSE sequence allows to obtain consistent values (*i.e.*, the difference in the calculation of *D* using different ^{1}H nuclei of the same molecule is well below the experimental error). The NMR-derived *D* values can be inserted in the Nernst-Einstein (NE) equation to obtain the related conductivity.

By employing a set of the described complementary techniques, such as thermodynamic measurements, vibrational spectroscopies, NMR spectroscopies, and computational methods, we found that the usually adopted Nernst-Einstein-based approach is not associated with the direct determination of the ionicity nor proton transfer. Nevertheless, considering the diffusion coefficients of anions, cations, and acidic protons, a qualitative conclusion is achieved. Our results prove out of any doubt that the correct interpretation of experimental results is of vital importance to account for not-quantitative proton transfer in protic ionic liquids. Finally, we introduce the new concept of Reduced Ionicity, a quantity explicitly accounting for both ionicity (defined as non-paired ions in the system) and the proton transfer extent.

Results and discussion

Thermal characterization

The DSC and TGA of the three formed compounds, collected to determine each PIL's characteristic temperatures, are summarized in Table 1. First, the decomposition temperature was determined to identify the temperature range in which the stability of the system was not threatened. All following characterizations were planned accordingly. Figure 1 depicts the obtained results. Although some sources indicate the ILs decomposition to start at the temperature where the mass loss is 3% (T'_d), a better approach consists of taking the minimum of the TGA derivative curve as the decomposition temperature (T_d). For the sake of comparison with literature data, we report the values

obtained with both approaches in Table 1, but the discussion will be based on the values obtained with the derivative method (DTGA).

TFA anion appears to lead to the least stable PIL (TEATFA), with a T_d of 478 K. This is due to the occurrence of the anion decarboxylation as previously reported at considerably higher temperatures for the pure acid[75]. Such a decomposition path leads to the complete loss of the sample, as witnessed by the absence of any residual mass.

TEAMS is more stable exhibiting T_d at 485 K. This PIL shows more than a single degradation process, which can be ascribed to TEAMS' multi-step decomposition and its thermolysis residuals. The most stable PIL is certainly TEATfO showing a T_d of 669 K. The analysis of the DTGA curve shows that TEATfO is also decomposing through a multi-step process similar to TEAMS. However, fluorination enhances the stability of the whole compound (with a residual mass at 800 °C higher than 20%). Indeed, TfO-based ILs are known to be thermally stable and are also used in fuel-cells[25,76]. The stability order interestingly follows the parent acid strength – TEATfO > TEAMS > TEATFA. Although some sources link the thermal stability to the extent of proton transfer[74,77,78], other evidence [79,80] highlighted that there is no direct correlation between the two properties, and caution is advised, especially when good leaving groups (*e.g.,* CO_2) are involved.

The phase transition temperatures of the PILs were investigated via DSC (Figure 1). At first glance, it appears that all three PILs can be extensively super-cooled, showing crystallization temperatures (T_c) well below their melting temperatures (T_m). The same was also observed while manipulating the samples for the analysis. All of them appeared solid at room temperature, but they melt after heating at 80 °C, remaining liquid upon storage at 20 °C for several weeks if left undisturbed in a vacuum desiccator.

According to the DSC curves in Figure 2b, TEATFA only shows T_c at 253 K and T_m at 294 K, with no sign of glass transition (T_g) in the examined range. TEAMS shows the T_g at 188 K in addition to the T_c at 266 K and T_m at 308 K, while TEATfO shows T_g, T_c, and T_m at 221 K, 247 K, and 305 K, respectively.

The wide distribution of literature values[16,37,74,79–84] and the discrepancy with our findings could be explained considering the different water content in the range 1 ppm[16] - 2%$_{mol}$[74] for TEAMS and TEATfO, and 50 ppm[37] - 4200 ppm[79] for TEATFA. Sometimes, though, the water content is not even reported. Indeed, it is well known that even small differences in water content could have dramatic effects on IL properties, especially in PILs[85].

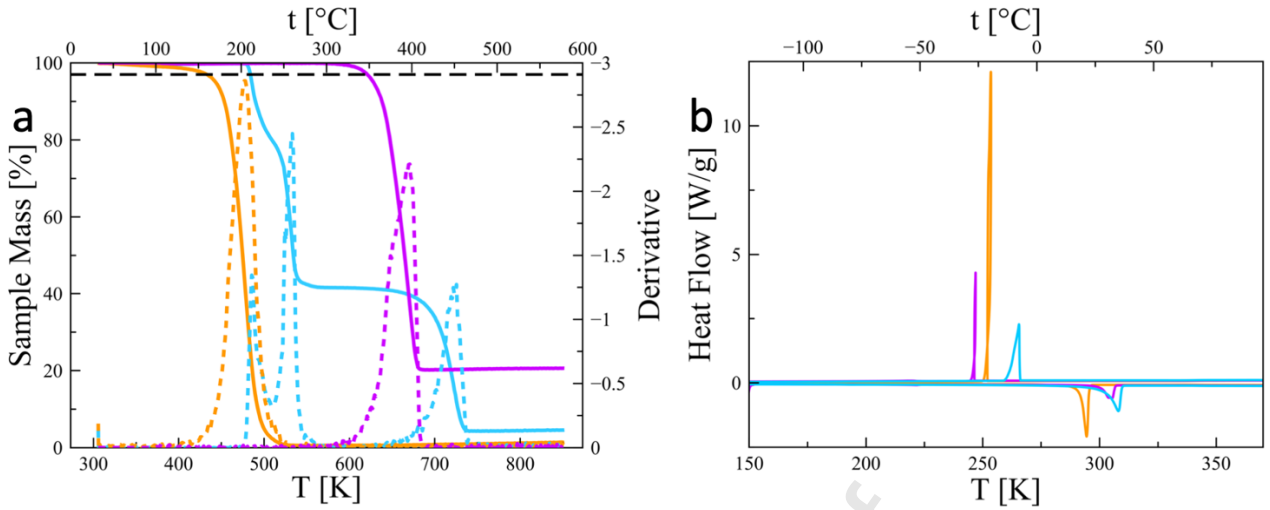

Figure 1: (a) TGA (solid lines) and DTGA (dashed lines) collected (heating rate: 5 K min^{-1}) of TEAMS (cyan), TEATFA (orange), TEATfO (purple). The black dashed line corresponds to the 3% mass loss threshold. (b) DSC curves (heating rate: 5 K min^{-1}) of TEAMS (cyan), TEATFA (orange), TEATfO (purple)

Table 1: Comparison of thermal characterizations of this work (underlined) and literature. All values are expressed in Kelvin.

	T_c	T_m	T_g	T'_d	T_d
TEAMS	265.53	308.03	187.68	484.25	485.52
	241.55[81]	297.45[81]	194.25[81]		578.15[37]
	249.15[37]	306.15[37]	211.05[33]		491.15[74]
	242.15[74]	306.15[82]	176.65[16]		498.15[83]
	250.25[80]	298.15[74]	198.15[82]		542.85[16]
		290.55[83]			476.15[80]
		294.75[16]			563.15[82]
		306.25[80]			
TEATFA	253.50	294.47	--	433.06	478.08
	231.15[37]	275.15[37]	190.15[37]		463.15[37]
	231.75[79]	281.75[79]			459.45[79]
TEATfO	246.97	305.34	221.26	620.56	657.55
	253.15[37]	303.15[37]	215.15[37]		649.15[37]
	260.15[74]	299.15[74]	215.15[84]		595.15[74]
	243.85[80]	307.45[83]			631.15[83]
		306.35[80]			585.65[16]
		307.15[82]			588.55[80]
		309.15[84]			653.15[84]
					663.15[82]

Anyhow, our results fit in the general trend already reported. Shmukler *et al.*[79] proposed a correlation between T_c and T_m for a series of triethylammonium-based PILs, including the three under investigation here, but we do not find anything similar. Again, the samples' different water content and thermal history could have a substantial effect on the observed thermal properties.

Conductivity and Viscosity

The study of PILs transport properties offers a deep insight into their nature; therefore, conductivity and viscosity measurements were carried out on all samples as a function of

temperature (Figure 2). The experimental data clearly show Vogel-Tamman-Fulcher (VTF) behavior in both cases, markedly deviating from linearity in the Arrhenius plot (log φ vs. 1000/T, in Figure S1). Thus, data were fitted with the equation:

$$\varphi(T) = \varphi_\infty \exp\left[-\frac{\xi_a^\varphi}{k_\mathrm{B}(T - T_0)}\right] \quad (4)$$

where φ is either the conductivity (σ) or the viscosity (η), φ_∞ is the value of that property at infinite temperature, ξ_a^φ is a parameter which is linked to the activation energy E_a^φ by $E_a^\varphi = |\xi_a^\varphi|$, k_B is the Boltzmann constant ($8.62 \cdot 10^{-5}$ eV K^{-1}), *T* is the absolute temperature, and T_0 is the temperature of zero configurational entropy, often referred to as the "ideal glass-transition temperature". A comparison with literature data is given in Table 2, while Equation 4 parameters are listed in Table 3. It is interesting to note how TEATFA is both the least viscous and the least conducive PIL. However, such a counter-intuitive behavior is difficult to justify only accounting for its low ionicity intended as "pronounced ion-pairing". If this were the case, the sample viscosity would have been higher due to the strong coulombic and hydrogen-bonding forces between the ions. A more profound interpretation must consider the IL's incomplete formation, resulting in a limited amount of charge carriers (explaining the low conductivity), accompanied by a reduced viscosity coming from the unreacted precursors (explaining the low viscosity). The presence in the TEATFA system of pure triethylamine (0.345 mPa s at 25°C) and trifluoroacetic acid (0.813 mPa s at 25°C) is expected to cause a net decrease in the viscosity, but at the expenses of available charged species jeopardizing the conductivity. On the other hand, TEAMS appears to be by far the most viscous PIL but displays higher conductivity than TEATFA. Once more, the degree of IL formation plays a pivotal role in this PIL, too. Here, the surprisingly high viscosity is undoubtedly caused by the more pronounced ion formation being mesylic acid stronger than trifluoroacetic acid (*i.e.*, a higher proton transfer can be confidently assumed). As a consequence, the conductivity is higher, although the viscosity reduces ion mobility. Finally, TEATfO is, by a large margin, the most conductive PIL in the explored temperature range. The low coordinating power of triflate, together with the strength of the triflic acid, makes this result expected and in line with the literature[25,74,80,86]. Here, we could expect the PIL to be nearly completely formed. Passing to the VTF space, E_a^σ and E_a^η values for TEATFA are in excellent agreement with each other, suggesting that the conductivity in this system is dominated by viscosity, and other effects, such as ion-pairing, are not significant. Once again, this evidence hints at the incomplete formation of this particular IL. If the unreacted precursors are in significant excess, then the ion-pairing is statistically limited since the mixture would be more similar to a dilute salt solution rather than a proper ionic liquid. Consequently, the activation energies for the viscous and conductive fluxes converge, *i.e.*, once the charged species start moving, there is no additional energy required to break the ion pairs activating the conductive flux. For the other two ILs, E_a^σ is lower than E_a^η suggesting that for higher degrees of formation there is no need to activate the viscous flow to start the conductivity. In an ion-rich system, there is no need for the ions to move to carry charges, as they could make the charge "jump" from

one site to another by merely changing their solvation shells, *i.e.,* the hopping mechanism, with no need for viscous flow (As schematically depicted in Figure S2 in Supporting Information). However, this effect should not be confused with the Grotthuss mechanism, since no chemical reaction is involved in our case. It is worth noting that the opposite is observed in AILs, in which stable ion clusters jeopardize the conductivity. A widespread approach to qualitatively estimate the ionicity of the ionic liquids is the so-called Walden plot, which correlates the logarithm of the molar conductivity with the logarithm of the fluidity (η^{-1}). To obtain the molar conductivity, we extracted the ILs molarity from density measurements (shown in Figure S3) and applied the relation:

$$\Lambda = \sigma \cdot \frac{\mathrm{MW}}{\rho} \qquad (5)$$

where Λ is the molar conductivity, ρ is the density expressed in g dm^{-3}, and MW is the sample molecular weight. In the Walden plot, a reference ideal behavior line is represented by 1M KCl, which is considered fully dissociated and, thus, 100% ionic. A second reference line is usually displayed, assuming 10% ionization of the same 1M KCl solution. These references appear to be wholly arbitrary[63,65] and often poorly discussed in the literature, with some groups reporting the line being "0.01M KCl", some reporting "0.1M KCl" and others the (correct) "1M KCl". Moreover, the aqueous KCl system was selected as a reference only because it displays a nice correlation between molar conductivity and fluidity. Here we use the unambiguous definition of the ideal behavior line to be "the bisector passing through the origin of the Walden plot" (*i.e.,* solution of Equation 6 with α=1). For the 10% reference line, instead, we simply shift the ideal line down one order of magnitude on the y-axis, thus assuming that the conductivity is linearly dependent on the concentration, which might not be the case in ILs, but it helps to separate the Walden plot in well-defined regions. Systems lying in between these lines are qualitatively defined as "good ionic liquids". Should they fall above or below, then they would be considered super-ionic or poorly-ionic, respectively. In general, it is expected for any given system to obey the Walden rule[46]:

$$\Lambda\eta^{\alpha} = C \qquad (6)$$

C is a temperature-dependent constant, and α is called the decoupling constant, which corresponds to the Walden plot's slope. The vertical distance between the ideal line and the examined system is called ΔW. Applying[36] the relation:

$$I_W = 10^{-\Delta W} = 10^{-\log(\Lambda/\Lambda_r)} = \frac{\Lambda_r}{\Lambda} \qquad (7)$$

where Λ and Λ_r are the molar conductivity of the sample and the reference line, respectively, it is possible to estimate the Walden ionicity (I_W) of the system. From Equations 6 and 7, it appears evident that in the ideal case α=1 and ΔW=0, therefore we consider this specific case as our reference in the Walden plot. The results for the three PILs herein investigated are reported in Figure 2 and Table 4. All PILs lie below the ideal line, with TEATFA being just under the 10% I_W reference line, *i.e.*, it is classified as a poor-

ionic liquid, which is in complete agreement with our previous suggestion of a scarcely formed PIL. The other two PILs lie in between the two reference lines, thus behaving as good-ionic liquids, with TEATfO being the closest to the reference 100% dissociation line. On a more quantitative analysis, through the Δ*W* values and Equation 7, the Walden ionicity values are obtained and reported in Table 4. As expected, I_W values follow the order TEATfO>TEAMS>TEATFA. Some groups suggested a correlation between the Walden ionicity of protic ionic liquids and the ΔpK_a of the Brønsted precursors[43,64,77]. While this approach yields consistent results, it must be considered contingent because pK_a values are meaningful only in water (and in a few other solvents). Angell, though, has shown[87] how ΔpK_a is undoubtedly a valid rule-of-thumb to rationalize qualitative results such as Δ*W* values. The pK_a values for the precursors used in this work were found in the literature[88–91] and conveniently reported in Table S1. From a physical point of view, ΔpK_a is related to the free energy of the proton transfer from the acid to the base through:

$$\Delta G^0 = -RT\,\Delta \ln K_a = -2.303\,RT\,\Delta \mathrm{p}K_a \quad (8)$$

where *R* is the gas constant. It must be clear that Equation 8 is strictly valid only if the proton transfer happens in a 1M aqueous solution, as also specified by Angell himself[16]. The results obtained for our systems are reported in Table 4. A markedly negative free energy is found for all the three systems, hinting at a quantitative proton transfer, in open contradiction with all the other experimental results. We can, therefore, conclude that this approach is not giving reliable information on the considered PILs. The same is true considering the hypothetical protic ionic liquid triethylammonium acetate, with a ΔpK_a of ~6. By applying Equation 8, a ΔG^0 = -34.3 kJ mol^{-1} is obtained at room temperature, which points toward a quantitative proton transfer. On the other hand, the reaction does not quantitatively occur in reality, as mentioned earlier. Yoshizawa *et al*. proposed that a ΔpK_a>10 is required for complete proton transfer[64], which would rule out triethylammonium acetate, but would consider TEATFA a completely formed PIL, which is also not the case (*vide infra*).

As pointed out by Daviowski and coworkers[55], proton affinity differences (Δ*PA*) are more reliable than ΔpK_a to discuss Walden ionicity in pure ionic liquids. DFT calculations in the gas phase could return the proton affinity value for every protonated/non-protonated pair discussed[92]. The proton affinities for the PILs herein investigated are reported in Table S2, while the Δ*PA* values are listed in Table 4. Interestingly, the Δ*PA* for triethylammonium acetate is ~500 kJ mol^{-1}, in agreement with the experimentally observed non-quantitative formation of the ionic liquid.

A useful correction to the Walden plot was introduced by Bonhôte *et al.* [93] and then re-proposed by Abbott and MacFarlane [46,94]. It is based on the role played by the ion size on diffusion, clearly highlighted in the Stokes-Einstein equation (Equation 9). They introduced a correction factor ζ for the viscosity explicitly accounting for the ion sizes (Equation 10), and then use log ($\zeta\eta^{-1}$) in the Walden plot. Moreover, Equation 6 can be expressed as Equation 11[46], explicitly showing the ion-size dependency of the Walden rule.

Table 2: Conductivity [mS cm^{-1}] and viscosity [mPa s]. Data in this work (underlined) and in literature at 25 °C. Other temperatures and water content in brackets.

TEAMS	TEATFA	TEATfO
Conductivity		
<u>1.84 (76 ppm)</u>	<u>1.52 (52 ppm)</u>	<u>4.55 (61 ppm)</u>
1.91 (100 ppm)[81]	2.45 (420 ppm)[79]	27.6 (120 °C) (N/A)[83]
2.03 (2%$_{mol}$)[74]		4.79 (2%$_{mol}$)[74]
16.3 (120 °C) (N/A)[83]		
Viscosity		
<u>117.0 (76 ppm)</u>	<u>28.6 (52 ppm)</u>	<u>52.5 (61 ppm)</u>
94 (810 ppm)[80]		56 (500 ppm)[80]

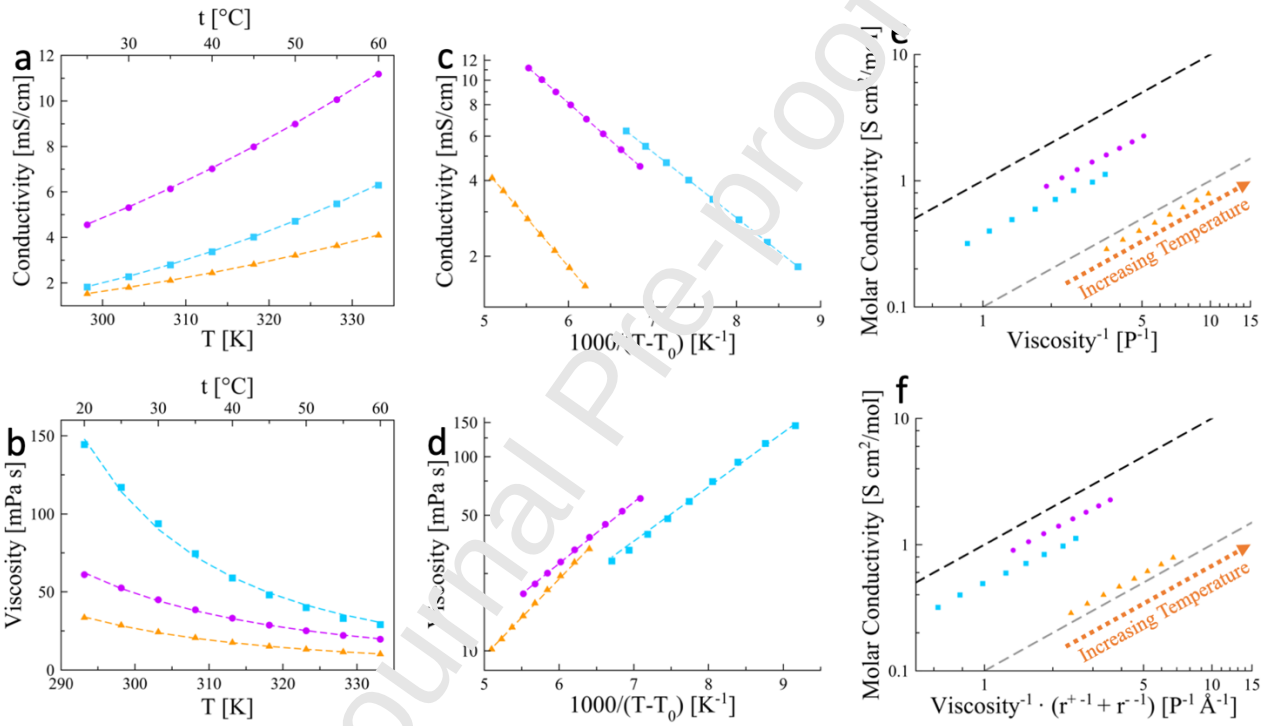

Figure 2: Conductivity (a) and viscosity (b) as a function of temperature. Panels (c) and (d) show the VTF plots of the same quantities, respectively. Data points (symbols), VTF fit (dashed lines). Walden plot (e) and Radii-corrected Walden plot (f). Reference lines for 100% dissociation (black) and 10% dissociation (grey). TEAMS (cyan squares), TEATFA (orange triangles), TEATfO (purple circles).

Table 3: VTF fitting derived parameters

PIL	Conductivity		
	σ_∞ [mS cm^{-1}]	E_a^σ [10^{-2} eV]	T_0^σ [K]
TEAMS	360±1	5.21±0.08	184±1
TEATFA	390±2	7.7±0.2	137±2
TEATfO	470±2	5.8±0.1	152±2
PIL	**Viscosity**		
	η_∞ [mPa s]	E_a^η [10^{-2} eV]	T_0^η [K]
TEAMS	0.41±0.06	5.6±0.1	184.0±0.2
TEATFA	0.098±0.004	7.87±0.06	137.0±0.1
TEATfO	0.35±0.02	6.27±0.06	152.0±0.1

$$D_i = \frac{k_B T}{f\,\eta\,r_i} \qquad (9)$$

$$\zeta = \frac{1}{r^+} + \frac{1}{r^-} \qquad (10)$$

$$\Lambda\eta^{\alpha} = C\left(\frac{1}{r^+} + \frac{1}{r^-}\right) \qquad (11)$$

In Equation 9, D_i and r_i are the diffusion coefficient and the hydrodynamic radius of the species *i*, respectively. The parameter *f* is a constant with a value of 4π for entirely slip boundaries and 6π for perfectly stick boundaries. In Equations 10 and 11, r^+ and r^- are the hydrodynamic radii of the cation and the anion, respectively. By applying the ζ correction factor, the result is a horizontal shift of the Walden plot points, usually leading to smaller $\Delta W'$ values[46] compared to the same quantity derived without accounting for ionic radii correction, as can be seen in Figure 2 and Table 4. The hydrodynamic radius of the ions was obtained as reported elsewhere[95]. The use of Ångstroms as units for the ion radii is completely arbitrary, but it should be noted that the same arbitrariness is found in the choice of centimeters for the molar conductivity and inverse Poise for the fluidity. The Walden plot is built as an empirical tool and, consequently, the most convenient units are adopted to return reliable and meaningful information.

By choosing the set of units [S cm^2 mol^{-1}] vs. [P^{-1} Å^{-1}], the I_W values obtained by Equation 7 are in good agreement with the values obtained with diffusion coefficients and Nernst-Einstein equation (*vide infra*). The similarities between the systems make the overall relative order to stay the same for the uncorrected Walden plot. Some critical difference, though, can be appreciated. Most notably, TEATFA now lies just above the 10% I_W threshold line, obtaining the status of good-ionic liquid, with a Walden ionicity of 11.8% obtained by Equation 7. As it will be more explicit in the following, the correction is capable of returning more reliable information than the classic approach. The linear fitting of the experimental data in the Walden plot readily yields α and log *C* (Equations 6 and 11), which are the slope and the intercept of the fitted line, respectively. For the three studied PILs, the fitting parameters are shown in Table 4. The value for α is the same, being the correction just a horizontal shift. On the other hand, the intercepts are markedly different for the bare (*C*) and corrected (*C'*) plots.

Extrapolating the lines obtained by the fitting to η^{-1}=0 (*i.e., infinite* viscosity) when both the axis in the Walden plot are expressed in linear scale, one obtains the conductivity at *infinite* viscosity ($\Lambda_{\eta\infty}$ in Table 4), which can be interpreted as resulting from the purely hopping ion movement, being any diffusion-driven conductivity wholly frozen. TEATFA shows the lowest $\Lambda_{\eta\infty}$ values by a large margin, which is explained by the anion's geometry. It is meaningless to define a $\Lambda'_{\eta\infty}$ including the radii-correction since the intercept at η^{-1}=0 is unaffected by any multiplicative correction on the x-axis. TFA anion can build, in its direct surroundings, a 2D network of hydrogen bonds since the two carboxylic oxygen atoms lie in the plane. On the other hand, the triflate and mesylate anions have an additional oxygen atom pointing out of the plane, resulting in a potentially 3D hydrogen-

bonded network. Moreover, the negative charge delocalized on two oxygen atoms makes TFA the most prone to form firmly bound ion pairs. In this landscape, the potential energy barrier for the hopping is markedly lower for TEATfO and TEAMS. The observed difference between these two can also be explained in terms of the coordinating character of the ions. However, the geometry and the coordination character are not the only properties contributing to the different behaviors. The proton transfer of the PILs is likely to play a pivotal role in all these observations. The same approach applied to aprotic ionic liquids would remove the uncertainty on the composition, thus returning a more solid base for further discussion.

Table 4: Walden plots-derived parameters and other ionicity indicators. Both ΔW and ΔW' are the one calculated at 25° C (the difference is minimal with other points)

	TEAMS	TEATFA	TEATfO
α	0.884	0.975	0.932
C [S cm^2 mol^{-1}]	0.372	0.085	0.499
C' [S cm^2 mol^{-1}]	0.490	0.122	0.693
$\Lambda_{\eta\infty}$ [S cm^2 mol^{-1}]	0.074	0.013	0.107
ΔW	0.426	1.078	0.24
I_W [%]	37.5	8.4	5.[illegible]
$\Delta W'$	0.322	0.928	0.183
$I_{W'}$ [%]	47.6	11.8	65.6
ΔpK_a	12.7	10.6	24.8
ΔG^0 [kJ mol^{-1}]	-72.5	-60.[illegible]	-141.6
ΔPA [kJ mol^{-1}]	381.8	388.[illegible]	298.3

Raman Spectroscopy

Qualitative insight into the nature of the interactions in bulk PILs is provided by Raman spectroscopy. The presence of specific functional groups in the compounds and the different symmetry of the precursor Brønsted acid and its anionic conjugated base could shed light on the composition of the three PILs. In order to have a reliable set of references, the spectra of the pure precursors, the 1M aqueous solutions of each acid potassium salt, and triethylammonium chloride were also collected. In this way, it is possible to obtain the experimental spectra of the single ions since the monoatomic counter-ions K^+ and Cl^- have no vibrational contribution. The solutions were diluted enough to avoid strong coupling between the ions. The collected data are plotted in Figure 3.

The band assignment, performed with the aid of DFT calculations, is reported in Supporting Information along with the calculated spectra (Figure S4). The spectra of all PILs are very well reproduced by the superposition of those from the cation and the anion, as can be expected for fully formed ionic liquids. However, some characteristic bands are identified (see Table 5), which could differentiate between ions and precursors. It is interesting to note that the point group of symmetry changes only for the pairs HMS/MS^- and HTfO/TfO^- passing from C_s to the more symmetric C_{3v}. The HTFA/TFA^- pair is always in the C_s group,

while TEA/HTEA$^+$ is in C_3, regardless of the protonation. These small molecular symmetry changes generate little-to-none modifications of the selection rules for the system's active normal vibration modes. Nevertheless, for all the anions, a band emerging from the deprotonation is easily tracked to witness the IL formation. The proton transfer activates the anti-symmetric stretching modes of the carboxylic (~1435 cm^{-1}) and sulfonic (~1040 cm^{-1}) functional groups. Unfortunately, there is no signal coming unambiguously from the Brønsted precursors, which would have allowed a quantitative determination of the ILs' proton transfer.

Nonetheless, PILs are formed to some extent because of the anions' anti-symmetric stretching peak presence in the spectra of the samples. A closer look at the TEA/HTEA$^+$ δ_{hch} mode peak (Figure S5), though, hints again to the not complete formation of TEAMS and TEATFA. This feature appears to be distinctly asymmetric for these two compounds, clearly showing a shoulder at lower wavenumbers. Comparing the PIL spectra with those of pure triethylamine and the 1M solution of triethylammonium chloride (Figure S5), it can be concluded that there is a non-negligible amount of the precursor Brønsted base (and, consequently, the acid) which has not reacted and remained in the system. These results correlate well with those from Infrared and NMR spectroscopies (*vide infra*). Focusing on TEATFA, the ν_{CC} band between 770 cm^{-1} and 870 cm^{-1} is diagnostic of the formation of the anion for acetate-based systems, as shown by Umebayashi *et al.*[22,24] Specifically, in the case of dissociation, the signal is substantially red-shifted if compared to the pure acid one. Figure S6 reports the specific Raman region for the TEATFA system. As reported earlier[22], the fingerprint of unreacted acid is clearly observed in the spectra.

Albeit the signal in TEATFA is red-shifted compared to HTFA, it is at lower frequencies if compared with the KTFA 1M solution.

In order to exclude the possible influence of different solvation shells and dielectric constants, a system composed of TEATFA 67%$_{vol}$ and HTFA 33%$_{vol}$ was prepared, and its Raman spectrum was collected. The comparison shows that the broad, asymmetric signal at ~830 cm^{-1} in TEATFA is due to unreacted acid rather than the anion. The pronounced blue-shift compared to pure HTFA can be explained in terms of different dielectric constants and solvation shells.

Far Infrared Spectroscopy

The Far Infrared (FIR) region of the vibrational spectra carries essential information regarding the hydrogen bond features. In particular, the band between 100 and 200 cm^{-1} is characteristic of the inter-species hydrogen bond stretching in PILs, as widely reported in the literature[27,52,96–100]. TEAMS and TEATfO have already been studied by Ludwig *et al.*[53] using FIR along with TEATFSI, including different deuteration degrees. These authors correlated the interionic peak position with the hydrogen bond binding energy, but they also state, "However, this relation was obtained by assuming that the full masses of anions and cations are involved in the vibrational motion. If that is not the case, deviations from the given relation can be expected", thus assuming that the PILs are completely formed, and the band originates solely by the interaction between the ions. The evidence herein reported are, however, point to a different direction, *i.e.*, a more complex system where

different hydrogen-bonding species coexist and potentially contribute to the observed FIR band. DFT calculations show, indeed, that dimers of all three acids have active normal modes of vibration in that region, arising from the anti-symmetric HB stretching (see Figure S7). Figure 3 reports the FIR spectra of TEAMS, TEATFA, and TEATfO collected as a function of temperature.

Albeit the signal in TEATFA is red-shifted compared to HTFA, it is at lower frequencies if compared with the KTFA 1M solution. In order to exclude the possible influence of different solvation shells and dielectric constants, a system composed of TEATFA 67%$_{vol}$ and HTFA 33%$_{vol}$ was prepared, and its Raman spectrum was collected. The comparison shows that the broad, asymmetric signal at ~830 cm^{-1} in TEATFA is due to unreacted acid rather than the anion.

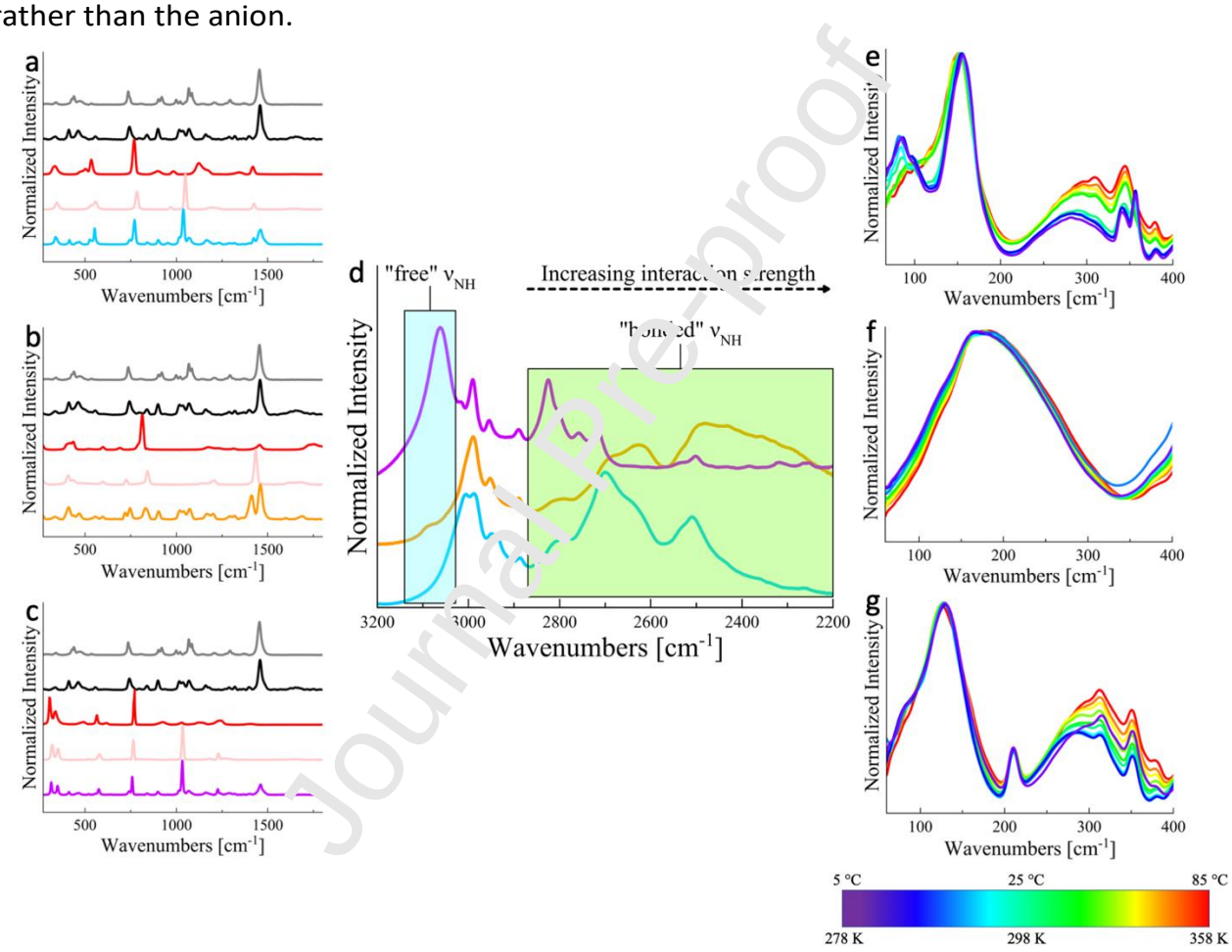

Figure 3: (a-c) Raman spectra at 25 °C of (a) TEAMS (cyan), TEATFA (orange), TEATfO (purple). In panels a-c (from top) pure triethylamine (grey), 1M aqueous triethylammonium chloride (black), pure corresponding acid (red), 1M aqueous potassium salt of the corresponding acid (pink). (d) X-H stretching region of Mid Infrared spectra at 25 °C. The boxes highlight specific stretching modes. From top TEATfO (purple), TEATFA (orange), TEAMS (cyan). (e-f) Far Infrared spectra as a function of temperature. (e) TEAMS, (f) TEATFA, (g) TEATfO. The temperature is indicated by the color bar.

Table 5: Normal modes selected as a probe for ionic liquid formation.

TEA/HTEA$^+$		**HMS/MS$^-$**		**HTFA/TFA$^-$**		**HTfO/TfO$^-$**	
cm^{-1}	**mode**	**cm^{-1}**	**mode**	**cm^{-1}**	**mode**	**cm^{-1}**	**mode**

1455	δ_{hch}	1050	ν^{as}_{so}	1435	ν^{as}_{co}	1035	ν^{as}_{so}
--	--	--	--	830	ν_{cc}	--	--

As reported above, a shift towards lower frequencies for increasing temperature is observed for TEAMS and TEATfO. The explanation given in the literature accounts for the weakening of the hydrogen bond as the temperature is increased. On the other hand, TEATFA shows the opposite behavior, *i.e.*, its broad band shifts toward higher frequencies upon heating. This counter-intuitive trend could find an explanation considering once more the not complete formation of this PIL. The trifluoroacetic acid is the weakest among the three tested herein. ^{1}H-NMR spectroscopy investigation of TEATFA (*vide infra*) clearly shows a peak at ~11 ppm, which is more compatible with an acidic proton rather than an ammonium one. It is reasonable to consider that a non-negligible amount of the acid is still in the system on these bases. The heating of the IL below its decomposition temperature results in shifting the equilibrium towards the formation of TEATFA. These results are seemingly in disagreement with the literature [60,101], where an increased concentration of neutral species is found in the gas phase upon heating of the ILs. It must be noticed, though, that gas and liquid phases are intimately different. As a matter of fact, though, in the gas phase a charged species is vastly less stable than in the liquid phase, being the density of oppositely charged species (necessary to stabilize the ion) lower. Since the HB interactions in the PIL are stronger than the one between neutral species, the increased number of ions in the system explains the counter-intuitive blue-shift of the FIR band of this particular PIL upon heating. This interpretation would also explain the broadness of the FIR signal for this PIL, which results in the convolution of several different contributions, all active in a narrow spectral window. It is also worth noting that for TEAMS and TEATfO, it is possible to recognize the solid-to-liquid phase transition. Both PILs have a peak at <100 cm^{-1} (for TEATfO it is only a shoulder) at low temperatures, which gradually vanishes upon heating. For TEAMS, also the peak at ~360 $cm^{-1,}$ which is visible at lower temperatures, abruptly vanishes as the system liquefies. These normal modes appear to be IR-active only in the solid-state, which can be explained with a specific symmetry breaking. We are currently working to determine the crystal structure of these compounds to clarify this and other observations. Others have suggested[102] that the hydrogen-bond characteristic signal in PILs may be deconvoluted into ion-ion mode and precursor-precursor mode. While it is conceptually a valid point, caution is advised in applying such a simplistic approach. The presence of precursors in non-negligible amounts would induce a plethora of different hydrogen-bonded pairs. Cation-anion and acid-base interactions are positively contributing, but one must also consider the effect of cation-base, cation-acid, anion-acid, and acid-acid even in the simplest case of a single hydrogen-donor and a single hydrogen-acceptor. Not to mention possible collective motions and (hindered) rotational modes that could impact this very low-frequency region of the spectrum.

Infrared spectroscopy

We employed infrared spectroscopy to check for the formation of the ammonium functional group because, in the specific case of triethylammonium cation, the N-H stretching (ν_{NH}) appears to be Raman-inactive[103] in our experiments (Figure S8). In the region around 3000 cm^{-1}, a plethora of active X-H stretching modes are active in the examined systems, but a general trend is pointing towards a poorly-formed and highly-associated ionic liquid in the case of TEATFA is emerging. In particular, the ν_{CH2} signal is the highest frequency normal mode found in pure triethylamine (~2975 cm^{-1}), according to the NIST database[104]. In the three PILs, the corresponding peak is clearly observed at ~2988 cm^{-1}, ~2990 cm^{-1}, and ~2990 cm^{-1} for TEAMS, TEATFA, and TEATfO, respectively. Interestingly, an evident band splitting is found for this vibrational mode for all three samples. The analysis of this feature is beyond the scope of the present work, but a tentative interpretation is the presence of different triethylammonium conformers in the system. The proton transfer on the nitrogen, though, generates another additional signal at higher frequencies for TEATfO and, to a much minor extent, TEATFA. This peak is attributed to poorly-interacting (or "free") ν_{NH}[80], whereas the complex superposition of signals in the 2200-2850 cm^{-1} region is also assigned to ν_{NH}, but with the proton interacting with the surroundings[80]. A strong endorsement for this assignment comes from the complete absence of signals in both regions in the Raman spectra. It is known that secondary amines[103] (and, by extension, tertiary ammonium ions) show no ν_{NH} signals, having the N-H stretching only a very small Raman cross-section due to the low change in the polarizability ellipsoid during the vibration. The strength of the interaction is inversely proportional to the wavenumber of the vibrational mode. TEATfO shows a clear, well-defined, and intense peak at ~3062 cm^{-1}, and TEATFA has a low but recognizable bump at ~ 3088 cm^{-1}. TEAMS seems not to display the "free" ν_{NH} peak, consistently with our other observations, which point towards strong ion-pairing in this protic ionic liquid. Considering TEATfO, it is safe to say that the ionic liquid is extensively formed and that most of it is not engaged in ion-pairing, as expected for the low-coordinating triflate anion. Conversely, TEAMS appears to be also markedly formed, with most ions hydrogen-bonded. TEATFA shows a minimum contribution for the "free" ν_{NH}, while a rich population of vibrational modes is found in the "bonded" ν_{NH} region. It is worth noting that N-H stretching modes usually have a high IR intensity, more pronounced than C-H modes. The fact that in TEATFA the ν_{NH} broad signals only barely overcome the ν_{CH2} points toward a small ammonium population. These observations advise caution when dealing with protic ionic liquids in assuming a priori a quantitative proton transfer.

NMR spectroscopy

Albeit NMR spectra could not unambiguously deduce quantitative information on the degree of PILs' formation, some meaningful conclusions could be drawn. The collected ^{1}H, ^{13}C, and ^{19}F NMR spectra are depicted in Figure 4.

Along with the spectra of the prepared PILs, the respective Brønsted precursors were also investigated to identify differences induced by the proton transfer. Interestingly, Davidowsky *et al.* [55] analyzed diethyl-methylamine-based PILs correlating the proton

affinity of the acid with the chemical shift of the acidic proton: indeed, the higher the former, the higher the latter. *PA* was preferred to pK_a since the latter is meaningful only in diluted environments. The ^{1}H NMR spectra reported here show a similar trend: the downfield shifted values here reported agree with the shielding effect of TEA. On this basis, we found an experimental confirmation of the actual proton transfer (*i.e.*, the formation of PILs), which, unfortunately, does not give us any quantitative hint on the extent of proton transfer. The acid-to-base proton transfer also influences the chemical shift of -CH_2- and -CH_3 groups of the formed ammonium cation ($HTEA^+$) compared to pure TEA. Indeed, a shift at higher ppm values is evidenced for the -CH_2- group, whereas the resonance frequency of the -CH_3 group is only slightly influenced by the proton transfer, as it could be expected considering the distance of the terminal methyl groups from the localized net positive charge on the nitrogen atom. For the methylene group, the chemical shift follows the order TEATFA > TEAMS > TEATfO, according to a previous report[35]. This trend seems to be counter-intuitive, being the smallest shift brought about by the strongest acid. However, one should consider that in a neat PIL, the cation is not isolated but rather surrounded (if not closely paired) by anions, leading to a further modification of the resonance frequency experienced by the methylene protons. The observed trend is in agreement with the anion coordination power. The signal related to the methyl group of the anion in TEAMS slightly shifts towards lower ppm values than pure HMS due to the acid "deprotonation". Regarding ^{13}C spectra, the effect of proton transfer is reflected in the de-shielding of methylene carbon (in α position to the protonation site), following the order TEATfO > TEAMS > TEATFA. The analysis of ^{19}F is more puzzling, being the chemical shift is predominantly influenced by the paramagnetic shielding rather than the diamagnetic one[105] in this case. Very unexpectedly, the fluorine atom of both HTFA and HTfO resonates at an almost identical frequency. A tentative explanation considers the sum of two factors: on the one hand, the sulfonate group has a higher electron-withdrawing character; on the other, the $HTFA^+$ forms more persistent dimers implying a larger fraction of the negative charge delocalized on the fluorine atoms. Once the PIL is formed, the ^{19}F signal of TEATfO shifts towards more negative chemical shifts, whereas for the TEATFA the opposite behavior is observed.

As stated above, focusing on the mere chemical shift could be misleading; yet, some interesting information could be extracted by comparing the PILs and the diluted aqueous solutions of the corresponding acids (see Figure S9). It should be kept in mind that the acids are entirely deprotonated if their molar fraction in water is lower than 0.4[106] (*i.e.*, 100 times more concentrated than our aqueous solution). Consequently, the obtained spectra are representative of the anions and not the corresponding acids. ^{19}F spectrum of TEATfO is almost entirely superimposed to that of TfO^-, whereas the spectrum of TEATFA appears 0.8ppm down-shifted compared to TFA^-. This inconsistency can be tentatively ascribed to two different factors: (i) an incomplete formation of the PIL, being the ^{19}F signal a mediated value between pure TEATFA and $HTFA^+$; (ii) the instauration of intermolecular interactions directly involving F atoms.

A verdict on this point (and more generally on NMR analyses) is far beyond the purpose of the present work, but it will be discussed in the second part of this manuscript, where we consider NMR to prove the formation of the PILs experimentally.

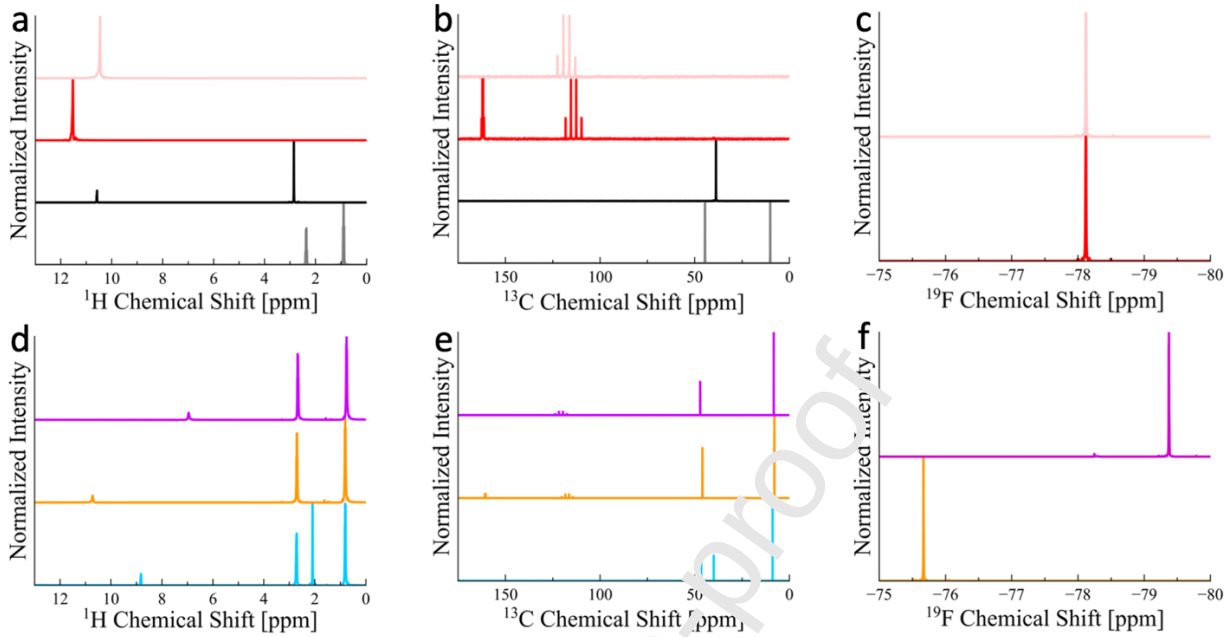

Figure 4: NMR spectra collected injecting the sample and the deuterated solvent in two separate concentric tubes at 25 °C. The panels a-c refer to the Brønsted precursors, panels d-f refer to the ionic liquids. ^{1}H-NMR (a, d), ^{13}C-NMR (b, e), ^{19}F-NMR (c, f). From top triflic acid (pink), trifluoroacetic acid (red), mesylic acid (black), triethylamine (grey) (a-c); from top TEATfO (purple), TEATFA (orange), TEAMS (cyan) (d-f).

Ionicity vs. Reduced Ionicity

PGSE-NMR (Pulsed-Gradient Spin-Echo NMR) is the technique of choice when the investigated systems contain NMR-active nuclei. In our case, both the anion and cation of TEAMS are easily probed via ^{1}H NMR. On the other hand, TEATfO and TEATFA are studied by means of ^{1}H-NMR (cation) and ^{19}F-NMR (anion). The selected peak decay is fitted with the function of Wu *et al.* [67] reported in Equation 12:

$$\ln(I_g) = \ln(I_0) - (\gamma\delta g)^2 D\left(\Delta - \frac{\delta}{3}\right) \quad (12)$$

where *Ig* is the signal intensity when a field with gradient *g* is applied, I_0 is the signal intensity for *g*=0, *γ* is the gyromagnetic constant, *Δ* is the diffusion delay time, *δ* is the duration of the gradient pulse, and *D* is the desired self-diffusion coefficient.

The gradient is calibrated using a pure D_2O sample, where the diffusivity of HDO in D_2O is calibrated to $1.9*10^{5}$ cm^2s^{-1} at 298 K. The diffusion coefficient of the cations and unreacted TEA, if present, are measured on both methyl ($-CH_3$) and methylene ($-CH_2$) peaks. These give roughly the same *D* value, and the values reported in Table 6 are averages of the two peaks. Concerning TEAMS, the *D* of the cation (and/or HMS) is measured on the methyl peak. Regarding TEATfO and TEATFA, being both the anions proton-free, the *D* values are measured for the fluorine peak by means of 2D ^{19}F NMR. The determined self-diffusion

coefficients as a function of temperature are listed in Table 6 (separated in anion and cation) and displayed in Figure 5 (summed).

The Stokes-Einstein relationship (SER, Equation 9) is widely employed to relate viscosity and diffusion coefficients. It has some severe limitations, though, which prevent its application in pure ionic liquids.

In particular, for SER to be valid (i) the investigated system must be a solution (*i.e.*, the solvent in significant excess of the solute), (ii) the radius of the solute must be substantially larger than the radius of the solvent, and (iii) the system must be dynamically homogeneous. On these bases, and considering the structural heterogeneity of many ILs[2,11,112,113,18,30,99,107–111], it is already clear that pure ionic liquids fail to meet all requirements.

Table 6: PGSE-NMR determined self-diffusion coefficients for the anions and cations as a function of temperature

	TEAMS [10^{-11} m^2 s^{-1}]		**TEATFA** [10^{-11} m^2 s^{-1}]		**TEATFO** [10^{-11} m^2 s^{-1}]	
t [K]	Cation	Anion	Cation	Anion	Cation	Anion
298	1.11 ±0.01	1.47 ±0.02	2.47 ±0.03	1.63 ±0.02	2.00 ±0.02	1.17 ±0.01
303	1.26 ±0.02	1.59 ±0.06	2.57 ±0.05	2.08 ±0.05	2.14 ±0.02	1.41 ±0.06
308	1.42 ±0.03	1.82 ±0.05	2.99 ±0.06	2.4 ±0.2	2.35 ±0.03	1.8 ± 0.1
313	1.68 ±0.04	1.94 ±0.07	3.30 ±0.06	2.8 ±0.4	2.64 ±0.04	2.1 ±0.1
318	1.99 ±0.05	2.26 ±0.09	3.40 ±0.09	3.2 ±0.4	2.71 ±0.05	2.4 ±0.2
323	2.43 ±0.07	2.63 ±0.07	3.70 ±0.09	3.7 ±0.3	2.95 ±0.06	2.7 ±0.2
328	2.70 ±0.08	2.9 ±0.1	3.90 ±0.09	4.1 ±0.4	3.22 ±0.08	3.0 ±0.3
333	2.8 ±0.1	3.0 ±0.1	4.1 ±0.1	4.4 ±0.4	3.49 ±0.08	3.3 ±0.3

Moreover, in the specific case of protic ionic liquids, one must also consider their different proton transfer, which also depends on the temperature. Therefore, an implicit boundary condition to the SER exists, *i.e.*, (iv) the ionic strength of the system must be constant with temperature. This condition is essential because a change in the PIL proton transfer would affect the radius of the moving species and enhance the dynamic heterogeneity by adding Coulombic interactions only in some areas of the system. The significant deviation of the investigated PILs from SER can be seen in Figure S10. Several corrections for SER have been proposed over the years, almost exclusively looking at different ways to define the hydrodynamic radius of the charged species[114]. As an example, Cheng-Li[115] correction (CLC) was explicitly developed for self-diffusion coefficients to overcome the (i) and (ii) limitations of SER. It considers the hydrodynamic radius to be:

$$r_i = \sqrt[3]{\frac{V_m}{N_A}} \qquad (13)$$

where V_m is the molar volume and N_A the Avogadro's number. While CLC returns good results for molecular liquids (usually within an error of 12%), it does not apply to ionic liquids because the molar volume depends on the specific configuration of the ion-pair, thus, in principle, being different for each one. Köddermann *et al.*[116] The leading cause for ILs deviations from SER is pointed at the dynamic heterogeneity, observing that if the IL is heavily diluted in a molecular liquid, the resulting system obeys SER. This finding is, though, expected because the system they obtained by dilution approached the requirements for SER to hold: (i) the new obtained system is a solution, (ii) the solvent used in their work was chloroform, which is markedly smaller than the IL investigated (namely, 1-ethyl-3-methyl-imidazolium bis (trifluoromethanesulphonyl) imide), (iii) the system is so diluted that any heterogeneity is averaged out. Their use of an aprotic ionic liquid also addressed the implicit fourth requirement on the proton transfer of the IL.

As a different approach, we introduce an empirically derived temperature-dependent correction factor (β) obtained using the PGSE-NMR derived diffusion coefficients in SER.

$$\beta = \frac{k_B T}{6\pi\,\eta\, r_i\, D_{NMR}} \qquad (14)$$

The correction factor β accounts for two physical phenomena of crucial importance in PILs: (i) the hydrodynamic radius of the diffusing species might significantly differ from those of the cations and anions themselves because of the possible aggregation driven by both Coulombic and aliphatic forces, and (ii) the partial formation of the ionic liquid generates regions with locally different microscopic viscosity, with low-viscosity domains where the Brønsted precursors are in excess existing along with high-viscosity parts where the IL is more concentrated. β values are shown in Table 7. As it appears clear from Equation 14, a system ideally follows SER for β =1. If β <1, the species in the system show a diffusion coefficient, which is larger than the one predicted by SER based on the macroscopic viscosity and the single-ion hydrodynamic radius. The opposite is true for β >1.

The effect of the correction parameter is then to adjust the quantity ηr_i to obtain effective viscosity and hydrodynamic radius. It is not possible to separate the two contributions because neither r_i nor the local viscosity are experimentally accessible. The obtained values show a marked dependence on the temperature, pointing towards the importance of the implicit requirement (iv). Moreover, especially for TEATFA, the higher the temperature, the larger than 1 is β, which rules out the hypothesis that changes in the effective r_i govern the deviation. In such a case, in fact, β should progressively become smaller (even smaller than one) upon increasing the temperature because clusters are expected to be destroyed at higher temperatures. Additionally, also the dynamic heterogeneity should be diminished by heating the system, but only if the sample composition remains constant at every temperature.

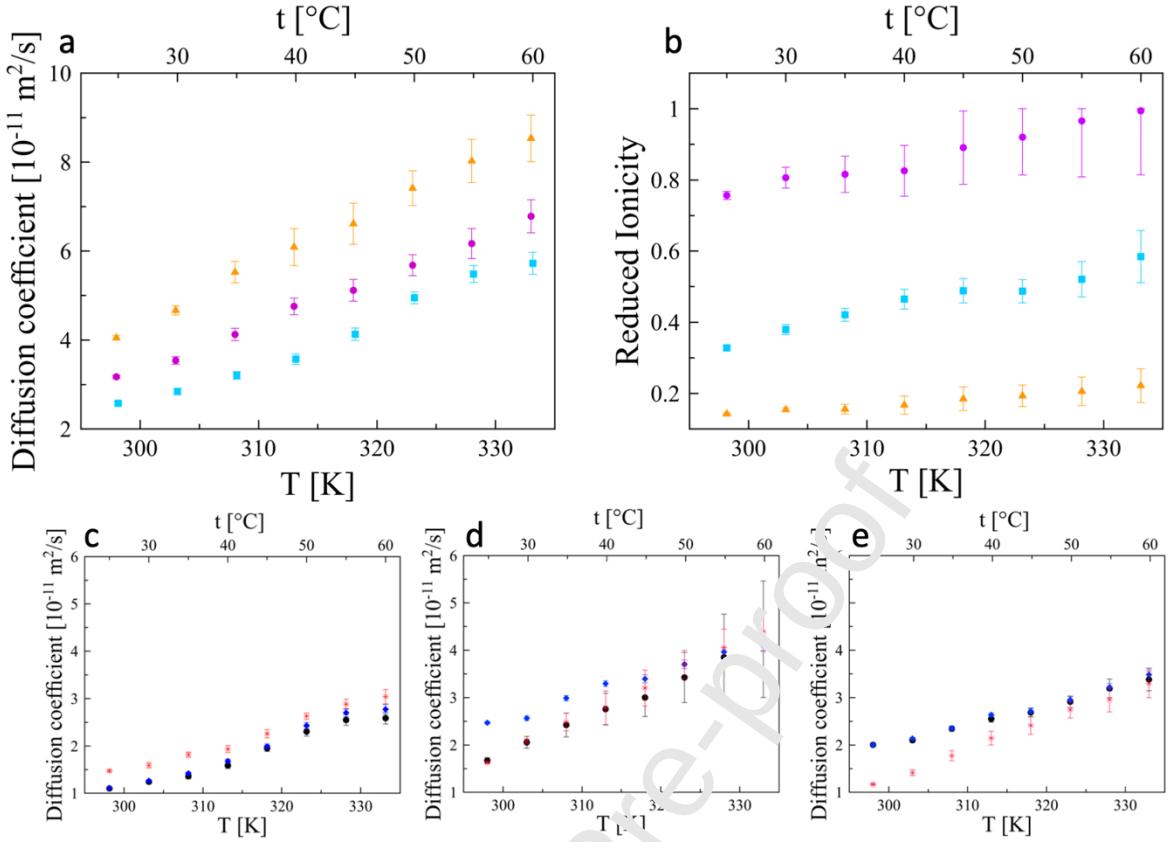

Figure 5: (a) PGSE-NMR derived diffusion coefficients. The values are the sum of the anion and cation diffusion coefficients at the given temperature. TEAMS (cyan squares), TEATFA (orange triangles), TEATfO (purple circles). (b) Reduced Ionicity derived from the ratio Λ/Λ_{NE}. TEAMS (cyan squares), TEATFA (orange triangles), TEATfO (purple circles). (c-e) Comparison between the diffusion coefficients of the acidic proton (black circles), anions (red stars), and cations (blue diamonds). TEAMS (c), TEATFA (d), TEATfO (e).

Table 7: Temperature-dependent empirical correction factor for the Stokes-Einstein relationship

	TEAMS		**TEATFA**		**TEATfO**	
t [K]	Cation	Anion	Cation	Anion	Cation	Anion
298	0.409	0.659	0.997	1.952	0.670	1.288
303	0.481	0.734	1.150	1.832	0.747	1.268
308	0.538	0.837	1.183	1.838	0.804	1.198
313	0.649	0.909	1.277	1.952	0.848	1.169
318	0.693	0.956	1.467	2.008	0.966	1.219
323	0.727	0.957	1.561	2.017	1.031	1.246
328	0.815	1.057	1.702	2.149	1.090	1.332
333	0.892	1.189	1.884	2.271	1.149	1.365

In our case, the proton transfer of the IL likely changes, generating more ions, which are responsible for more substantial viscosity variations. By plugging the PGSE-NMR derived diffusion coefficients in the Nernst-Einstein relationship (Equation 15), it is possible to

calculate the limiting molar conductivity, *i.e.,* the theoretical conductivity that a system would have if all the moving species were carrying a net electric charge.

$$\Lambda_{\mathrm{NE}} = \frac{N_{\mathrm{A}} e_0^2}{k_{\mathrm{B}} T} \cdot (D^+ + D^-) \qquad (15)$$

In Equation 15, Λ_{NE} is the theoretical molar conductivity. D^+ and D^- are the diffusion coefficients of the cation and the anion, respectively. Following the definition of Λ_{NE}, the ratio $\Lambda/\Lambda_{\mathrm{NE}}$ is a measure of the ionicity of the system. It should be once more clarified that the term "ionicity" for protic ionic liquids is ambiguous. Indeed, for aprotic ionic liquids, the term is used to address the degree of dissociation, *i.e.*, is a measure of the ion-pairing (Equation 1). For PILs, the scenario is more complicated because the proton transfer also contributes to the "loss" of ion conductivity, resulting in a smaller $\Lambda/\Lambda_{\mathrm{NE}}$ ratio.

Based on all the experimental and theoretical evidence above and to stop the dangerous confusion between ionicity and proton transfer/formation degree in protic ionic liquids, we propose the adoption of new terminology, introducing the concept of "Reduced Ionicity" (ι) which is directly linked to both *I* and *FD*. It is possible to express ι as a function of the concentration of all the species in the system, similarly to Equations 1 and 3:

$$\iota = \frac{[A^-] + [HB^+]}{[A^-] + [HB^+] + [A^-HB^+] + [HA] + [B]} \qquad (16)$$

By recognizing that $[A^-]=[HB^+]$ and that $[HA]=[B]$, it is possible to combine Equations 1, 2, and 16 to obtain a direct relationship between *I* and ι:

$$\iota^{-1} = I^{-1} \cdot K_{\mathrm{PT}}^{-1/2} \qquad (17)$$

It directly follows that, in general, for any ionic system regardless of its nature (*e.g.*, aprotic IL, protic IL, molten salt, aqueous solutions):

$$\frac{\Lambda}{\Lambda_{\mathrm{NE}}} = \iota \qquad (18)$$

contrary to what is usually reported in the literature, where the $\Lambda/\Lambda_{\mathrm{NE}}$ ratio is referred to as the ionicity of the system. Indeed, it should be clear that Equation 16 holds even if all the protonated species (HB^+, A^-HB^+, and HA) are exchanged with their aprotic counter-parts (B^+, A^-B^+, A). Equation 18 returns the ionicity only if the formation degree of the ionic species is 1, *i.e., [HA]=[B]*=0, or *[A]=[B]*=0, which is the same for aprotic ionic substances. Consequently, for PILs the term "ionicity" should not be used as it currently is because of the possible incomplete proton transfer (*i.e.*, formation degree), and the more general reduced ionicity should be used instead. By comparing Equations 1, 3, and 16 it is clear that *FD* is always higher than (or, at least, equal to) the reduced ionicity value, but the same is not true for ionicity. It is important noting the relationships in Equation 19.

$$\begin{cases} I \geq \iota \\ FD \geq \iota \end{cases} \quad (19)$$

The latter expression highlights why we adopted the term “reduced ionicity”, and shows how ι is a property fundamentally different from both *I* and *FD*. For example, in the case of a hypothetical PIL with *FD* << 1 (*e.g.,* TEAAc), it is quite possible that its ionicity (as defined in Equation 1) would be close to 1, because of the high dilution of the ions in the Brønsted precursors. On the other hand, some PILs with strongly coordinating ions (*e.g.,* chloride) could have *I* << 1 but *FD* (Equation 3) approaching 1. Both the systems in the examples would have ι << 1 (Equation 16), and a deeper insight on the system is needed to identify the reasons behind the observed value obtained by the Λ/Λ_{NE} ratio.

The results of this approach applied to the three PILs studied here are reported in Figure 5. For all the presented PILs, the reduced ionicity increases with the temperature, which is expected considering both the breaking of ion-pairs and the enhanced formation of ions themselves. As mentioned above, these values result from both paired ions and neutral molecules in the system, and a quantification of their relative weight is not possible only based on the obtained reduced ionicity values.

Nevertheless, it is worth pointing to a possible solution to this seemingly insuperable *impasse*. As shown above, MIR spectroscopy shows two distinct signals for "bonded" and "free" ν_{NH}, thus offering a chance to obtain the ionicity of the system in line with its standard definition of non-paired ions in the system. In the three proposed examples, though, the "bonded" ν_{NH} region is too complex to attempt a reliable quantification. We will give more insight into this direction in a forthcoming paper.

One final insight, and definitive proof of the incomplete formation of TEATFA, is granted by a closer look at the diffusion coefficient trends. PGSE-NMR enables obtaining the diffusion coefficients of whatever has a suitable NMR signal, meaning that any peak can be followed to determine the diffusion coefficient of the associated species. In Table 6, the coefficients for anions and cations are reported for all the PILs herein investigated. These values are compared in Figure 5, with the diffusion coefficient of the acidic proton, which always shows a clear peak in the ^{1}H-NMR of all the examined PILs. From Figure 5, it appears clear that the acidic proton diffuses bound to the amine in TEAMS and TEATfO, suggesting that the amine is the proton carrier, *i.e.*, the acid is deprotonated. Such a piece of evidence supports the substantial proton transfer in these two PILs. On the other hand, in TEATFA the proton essentially diffused with the CF_3 group, meaning that the acid is still mostly present in the system, confirming the incomplete proton transfer. At higher temperatures, the error bars for the acidic proton in TEATFA become too wide to give a robust interpretation of where the proton is. Such error bars could be seen as a hint to the increasing uncertainty on the proton position, which, at higher temperatures, can jump from the acid to the base more efficiently, increasing the IL proton transfer. All these pieces of evidence point at TEATFA being mainly composed of neutral species, TEATfO being a proper ionic liquid, and TEAMS being half-a-way between these two extremes. In this context, the reader is kindly invited to note how the superimposition of the ionicity

concept with the one of proton transfer could be safely done just for TEATfO, whereas other experiments are required to completely rule out the formation of tough ion-pairs in both TEATFA and TEAMS. However, it is interesting to note how the reduced ionicity values obtained in this rigorous way are in fair agreement with those extracted by the radii-corrected Walden plot, suggesting that tool as a reliable source of reduced ionicity values when PGSE-NMR cannot be used, even if with severe limitations[65].

Conclusions

To summarize, we reported the characterization of thermal, transport, and spectroscopic properties of three (plus one) triethylammonium-based protic ionic liquids with anions originated from acids of different strengths. This series was chosen as a proof of concept to discuss the intricate interplay between ionicity and proton transfer. The latter two concepts are too often confused with each other, and the effective degree of proton transfer is too easily overlooked, being considered quantitative. In this context, we aimed to investigate these PILs by means of different approaches to shed light on the ionicity/proton transfer interplay. We introduced the innovative concept of Reduced Ionicity for this scope and to end the ambiguity between ionicity and formation degree, accounting for both the phenomena. This quantity, and not the properly said ionicity, is what is obtained with the Λ/Λ_{NE} ratio (Equation 18).

Using several complementary techniques, we have demonstrated how the proton transfer in PILs is not always quantitative. The thermal stability follows the acid strength, with TEATfO being the most stable. On the other hand, the relatively low stability of TEATFA is due to the possible decarboxylation of the acid, which results in rapid evaporation of the whole compound. All the spectroscopy techniques used hint at the incomplete formation of TEATFA, but none of them was adequate to quantify the proton transfer. Nevertheless, the overall picture given by NMR and vibrational spectroscopies returns the information that at least some ionic liquid is formed in all the cases (Raman), that the degree of formation follows the order TEATfO>TEAMS>TEATFA (NMR), and that raising the temperature below the decomposition point increases the number of ionic species (FIR). MIR returns some (unexpected) concrete direct evidence of (i) the poor proton transfer in TEATFA (displaying only faint signals for the characteristic ν_{NH} vibrational modes), (ii) the sizeable proton transfer in TEATfO (intense peak of the characteristic ν_{NH} vibrational modes) and (iii) the meaningful aggregation experimented by TEAMS (ν_{NH} vibrational modes shifted toward lower wavenumbers). In order to obtain complementary evidence towards further enlightenment of proton transfer degree, the Walden plot remains a vital rule-of-thumb to classify these materials. However, the radii-based correction factor is confirmed to improve the reliability of Walden ionicity estimation vastly. In this regard, it should be noted how the Walden ionicity approximates the reduced ionicity and not the ionicity itself. The Walden ionicity calculated by the radius-corrected Walden Plot reasonably correlates with those measured by the more conventional and reliable approach based on comparing the experimental and Nernst-Einstein-derived conductivities. Overall, TEATfO can be considered a wholly-formed PIL (*i.e.*, $\iota = I = FD = 1$ in

the limit of relatively high temperatures). At the same time, a qualitative consideration can be drawn concerning TEAMS and TEATFA, having reduced ionicity values close to 0.6 and 0.2, respectively, at room temperature. While the values of diffusion and viscosity for TEAMS are compatible with a low reduced ionicity solely determined by ion-pairing, as firmly supported by the MIR spectra, the same is unlikely for TEATFA, for which we propose a substantial influence of the incomplete proton transfer. This conclusion is strongly supported by all the spectroscopic techniques used, particularly with MIR and the $1{:}2_{vol}$ acid:PIL Raman spectra, and by the fact that the acidic proton clearly diffuses with the trifluoracetic species in the PGSE-NMR experiment. Very interestingly, the diffusion coefficients calculated from the NMR analyses do not obey the Stoke-Einstein relation nor any of the radii-correction terms proposed over time. Thus, we contextually proposed an empirical correction factor, β, which accounts for local viscosity fluctuations and hydrodynamic radii changes. It should be pointed out that, albeit a definitive determination of ionicity and proton transfer was achieved only for TEATfO, we are confident that, quoting Agatha Christie, (more than) *three coincidences are a proof*: TEAMS has an almost quantitative proton transfer, but its reduced ionicity is jeopardized by ion-pairs formation, while TEATFA experimented a very low proton transfer being also prone to associating in ion clusters. In general, an IL can be considered pure if it is composed of at least $99\%_w$ of ions [117]. In the presented cases, only TEATfO and possibly TEAMS satisfy this criterion, with TEATFA most probably being a mixture of PIL and Brønsted precursors.
This work clearly shows that more (and different) approaches are required to shed light on the interplay between ionicity and proton transfer, a key topic in determining PILs' features, too often overlooked in the literature.

Methods

Materials

All materials were purchased at the highest degree of purity available and employed without further purification. Triethylamine ≥99.8% Merck, Triflic acid ≥99.5% T&J Chemicals, Mesylic acid ≥99.5% Merck, Trifluoroacetic acid 100% VWR Chemicals, Acetic acid ≥99.99% Sigma Aldrich.

Synthesis of the Ionic Liquids

The three PILs were prepared according to the following procedure. Triethylamine was poured into an ice-bath cooled, three-neck flask under dry nitrogen flow (1ml/min). A stoichiometric amount of the acid was then added dropwise under vigorous stirring over three hours. The flask was then removed from the cooling but left under stirring at room temperature over 12-16 hours. The final water content, determined by Karl-Fischer coulometric titration, was found in the range of 50-80 ppm for all three PILs.

Characterization

Thermogravimetric analysis (TGA) was performed using the TA Q5000 instrument. The sample was subject to a temperature ramp of 5 K/min under nitrogen flow.

Differential scanning calorimetry (DSC) measurements were performed using a TA Discovery DSC series with liquid N_2 cooling. First, the samples were heated up from room temperature to 350 K and then cooled down to 120 K. To allow full crystallization of the samples, *i.e.*, a more reproducible thermal behavior, sub-ambient annealing was performed by thermal cycling of the samples from 120 K to their cold crystallization temperature. Finally, the samples were cycled between 120 K and 373 K two times with a ramp of 5 K/min. For both TGA and DSC, the samples were filled in aluminum pans.

Density measurements were performed with an Anton Paar DMA 4500 M density meter.

Dynamic viscosity was determined with an Anton Paar MCR 102 rheometer, using a cone-plate geometry with a shear rate of 10 s^{-1}. Both the density meter and the rheometer are placed in a dry-room with a dew-point of 198 K.

The conductivity was determined in sealed glass conductivity cells (Materials Mates 192/K1) equipped with two platinum electrodes (cell constant of (1.0±0.1 cm)) using a thermostatic Bio-Logic conductivity meter.

Raman spectra were collected using the RAM II module of the Bruker Vertex 70v spectrometer, mounting Nd:YAG laser source (1064 nm) and a high sensitivity InGaAs detector. The samples were sealed in NMR tubes to prevent contamination. The signal was accumulated over 500 scans for each sample.

Far infrared absorption spectra were acquired using a Michelson interferometer (IFS66 V/S Bruker) working under low vacuum (2 mbar), equipped with a 6 µm thick mylar beam-splitter and DTGS detector. A Hg discharge lamp was used as a radiation source. A drop of the sample (30 µL) was incorporated between the Si windows of a commercial cell. The optical path length of the radiation was adjusted at 25 µm by a mylar spacer placed between windows. Reference spectra were collected without a spacer to avoid Fabry-Perot interference effects. In order to maximize the signal-to-noise ratio, 128 interferograms were accumulated, and their average was Fourier transformed using the Blackman-Harris apodization function (actual resolution 4 cm^{-1}). The absorption spectra were calculated via the Lambert-Beer law and pre-processed using the OPUS software.

Infrared spectra were collected with a Bruker Vertex 70v using a KBr beam-splitter and a DLaTGS detector. The samples were collected in the Attenuated Total Reflection (ATR) configuration on diamond crystals. The sample chamber was kept under vacuum (2 mbar) during the measurements. To enhance the signal-to-noise ratio the spectra and the background were collected 256 times and averaged.

All NMR spectra (^{1}H, ^{13}C and ^{19}F) were collected at 298 K with a 600 MHz JEOL ECZR spectrometer using a 5 mm Royal probe equipped with a z gradient coil producing a maximum gradient strength of 0.9 T m^{-1}. All samples reached thermal equilibrium before measurement. NMR measurements were made in coaxial tubes. The inner tube contains a deuterated solvent (required for lock) whereas the outer tube was filled with the investigated samples, allowing for a good signal-to-noise ratio. The aqueous solution was directly prepared in the NMR tube by diluting the pure acids (or TEA) to 0.1 mol L^{-1} in D_2O. The chemical shifts were referenced by setting to zero the standard chemicals, *i.e.,* TMS for ^{1}H and ^{13}C, $CFCl_3$ for ^{19}F.

Diffusion experiments on ^{1}H were acquired with a sequence characterized by encoding pulse duration, Δ of 4 ms, a diffusion time of 0.3 s, and 8 nominal gradient amplitudes, g, ranging from 80 to 800 mT m^{-1} chosen to give equal steps in gradient squared. DOSY experiments were recorded in a range of temperatures within 298 K and 333 K with an interval of 5 K, and all samples had reached equilibrium before measurement. Before performing DOSY measurement, for each temperature, the 90-degree pulse has been measured.

Diffusion experiments on ^{19}F were acquired with a sequence characterized by encoding pulse duration Δ of 5 ms, a diffusion time of 0.1 s, and 8 nominal gradient amplitudes, g, ranging from 80 to 800 mT m^{-1} chosen to give equal steps in gradient squared. DOSY experiments were recorded in a range of temperatures within 298 K and 333 K with an interval of 5 K, and all samples had reached temperature equilibrium before measurement. Before performing DOSY measurement, for each temperature, the 90-degree pulse has been measured.

Computational details

All computations were carried out using the Gaussian 09 program package[118] at B3LYP/6-311++G** level of theory. Starting geometries were built with Avogadro[119]. The geometry optimization was carried out before computing the intensities of vibrational frequencies. The calculated frequencies were assigned with the help of the VEDA software[120]. No imaginary frequencies were observed for any system, indicating the reaching of a real minimum of the potential energy surface. To account for biases arising from vibrational anharmonicity and rough treatment of electron correlation, a scale factor of 0.98 was employed to facilitate the comparison with experimental data[100]. The energetics of the acid deprotonation was studied through single-point energy at the same level of theory.

AUTHOR INFORMATION

Corresponding Authors

AM: alessandro.mariani@kit.edu;
SP: stefano.passerini@kit.edu

Author Contributions

All authors have given approval to the final version of the manuscript. AM and MB contributed to the same extent to the manuscript by conceptualization, interpretation of the results, and writing the manuscript. XG synthesized the PILs and collected DSC, TGA, conductivity, and viscosity data. AN supervised the FIR experiments. BC and NB performed 1H and 13C NMR measurements. RB and AB supervised the NMR experiments and performed 19F and PGSE NMR measurements. LG and SP edited the drafts and supervised the project.

Funding Sources

This research is partially supported by the Bundes Ministerium für Wissenschaft und Forschung (BMWi) research grant "FZK 03ETB003A HiFi-PEFC".

ACKNOWLEDGMENT

AM gratefully acknowledges Ms. Chiara Giovannini for the graphics of the Table of Contents, and Prof. Dr. Enrico Bodo, Dr. Francesca Leonelli**,** Dr. Ivana Hasa, Dr. Giovanni Appetecchi, and Dr. Luigi Bencivenni for the fruitful discussion. AM, XG, and SP acknowledge the support of the Helmholtz Association. LG acknowledges support from Regione Lazio, through Progetto di Ricerca 85-2017-15125 according to LR 13/08. All the authors gratefully acknowledge the reviewer for her/his valuable comments.

ABBREVIATIONS

^{13}C-NMR: carbon-13 nuclear magnetic resonance
^{19}F-NMR: fluorine-19 nuclear magnetic resonance
^{1}H-NMR: proton nuclear magnetic resonance
AIL: aprotic ionic liquid
ATR: attenuated total reflection
CLC: Cheng-Li correction
DEMA: diethyl methyl amine
DEMATfO: diethyl methyl ammonium triflate
DFT: density functional theory
DOSY: diffusion ordered spectroscopy
DSC: differential scanning calorimetry
DTGA: differential thermal gravimetric analysis
DLaTGS: deuterated lanthanum alanine doped triglycine sulfate
DTGS: deuterated triglycine sulfate
FD: formation degree
FIR: far-infrared
HAc: acetic acid
HB: hydrogen bond
HMS: methanesulfonic/mesylic acid
HTEA: triethylammonium
HTFA: trifluoroacetic acid
HTfO: trifluoromethanesulfonic/triflic acid
HTFSI: triflimidic acid
IL: ionic liquid
k_B: Boltzmann constant
KTFA: potassium trifluoroacetate
MIR: mid-infrared
MS: methanesulfonate/mesylate
MW: molecular weight

Nd: YAG: neodymium-doped yttrium aluminum garnet
NE: Nernst Einstein
NMR: nuclear magnetic resonance
PA: proton affinity
PGSE: pulsed gradient spin echo
PGSTE: pulse gradient stimulated echo
PIL: protic ionic liquid
pK_a: negative base-10 logarithm of the acid dissociation constant
ppm: parts per million
SER: Stokes-Einstein relationship
TA: thermal analysis
TEA: triethylamine
TEAMS: triethylammonium mesylate
TEATFA: triethylammonium trifluoroacetate
TEATfO: triethylammonium triflate
TEATFSI: triethylammonium bis (trifluoromethylsulfonyl) imide
TFA: trifluoroacetate
TfO: trifluoromethanesulfonate/triflate
TGA: thermal gravimetric analysis
TMS: tetramethyl silane
VEDA: vibrational energy distribution analysis
VTF: Vogel-Tamman-Fulcher

References

[1] T.L. Greaves, A. Weerawardena, I. Krodkiewska, C.J. Drummond, Protic Ionic Liquids: Physicochemical Properties and Behavior as Amphiphile Self-Assembly Solvents, J. Phys. Chem. B. 112 (2008) 896–905. doi:10.1021/jp0767819.

[2] T.L. Greaves, C.J. Drummond, Protic Ionic Liquids: Evolving Structure–Property Relationships and Expanding Applications, Chem. Rev. 115 (2015) 11379–11448. doi:10.1021/acs.chemrev.5b00158.

[3] A. Mariani, R. Caminiti, M. Campetella, L. Gontrani, Pressure-induced mesoscopic disorder in protic ionic liquids: first computational study, Phys. Chem. Chem. Phys. 18 (2016) 2297–2302. doi:10.1039/C5CP06800B.

[4] T. Welton, Ionic liquids: a brief history, Biophys. Rev. 10 (2018) 691–706. doi:10.1007/s12551-018-0419-2.

[5] D. Yalcin, C.J. Drummond, T.L. Greaves, Solvation properties of protic ionic liquids and molecular solvents, Phys. Chem. Chem. Phys. 22 (2019) 114–128. doi:10.1039/c9cp05711k.

[6] P. Walden, Ueber die Molekulargrösse und elektrieshe Leitfähigkeit einiger gazehmolzenen Salze, Bull. Acad. Imper. Sci St. Petersbg. 8 (1914) 405–422.

[7] R.D. Rogers, K.R. Seddon, Ionic Liquids - Solvents of the Future?, Science (80-.). 302 (2003) 792–793. doi:10.1126/science.1090313.

[8] F. Endres, S. Zein El Abedin, Air and water stable ionic liquids in physical chemistry, Phys. Chem. Chem. Phys. 8 (2006) 2101. doi:10.1039/b600519p.

[9] T.L. Greaves, C.J. Drummond, Protic ionic liquids: properties and applications., Chem. Rev. 108 (2008) 206–37. doi:10.1021/cr068040u.

[10] N.V.N. V. Plechkova, K.R.K.R. Seddon, Applications of ionic liquids in the chemical industry, Chem. Soc. Rev. 37 (2008) 123–150. doi:10.1039/B006677J.

[11] R. Hayes, G.G. Warr, R. Atkin, Structure and Nanostructure in Ionic Liquids, Chem. Rev. 115 (2015) 6357–6426. doi:10.1021/cr500411q.

[12] X. Gao, A. Mariani, S. Jeong, X. Liu, X. Dou, M. Ding, A. Moretti, S. Passerini, Prototype rechargeable magnesium batteries using ionic liquid electrolytes, J. Power Sources. 423 (2019) 52–59. doi:10.1016/j.jpowsour.2019.03.049.

[13] X. Gao, F. Wu, A. Mariani, S. Passerini, Concentrated Ionic-Liquid-Based Electrolytes for High-Voltage Lithium Batteries with Improved Performance at Room Temperature, ChemSusChem. 12 (2019) 4185–4193. doi:10.1002/cssc.201901739.

[14] X. Gao, X. Liu, A. Mariani, G.A. Elia, M. Lechner, C. Streb, S. Passerini, Alkoxy-functionalized ionic liquid electrolytes: understanding ionic coordination of calcium ion speciation for the rational design of calcium electrolytes, Energy Environ. Sci. (2020). doi:10.1039/D0EE00831A.

[15] X. Mao, P. Brown, C. Červinka, G. Hazell, H. Li, Y. Ren, D. Chen, R. Atkin, J. Eastoe, I. Grillo, A.A.H.H. Padua, M.F. Costa Gomes, T.A. Hatton, Self-assembled nanostructures in ionic liquids facilitate charge storage at electrified interfaces, Nat. Mater. (2019). doi:10.1038/s41563-019-0449-6.

[16] J.-P. Belieres, C.A. Angell, Protic Ionic Liquids: Preparation, Characterization, and Proton Free Energy Level Representation †, J. Phys. Chem. B. 111 (2007) 4926–4937. doi:10.1021/jp067589u.

[17] A. Idris, R. Vijayaraghavan, A.F. Patti, D.R. MacFarlane, Distillable Protic Ionic Liquids for Keratin Dissolution and Recovery, ACS Sustain. Chem. Eng. 2 (2014) 1888–1894. doi:10.1021/sc500229a.

[18] R. Hayes, S. Imberti, G.G. Warr, R. Atkin, Pronounced sponge-like nanostructure in propylammonium nitrate., Phys. Chem. Chem. Phys. 13 (2011) 13544. doi:10.1039/c1cp21080g.

[19] H. Ohno, Functional Design of Ionic Liquids, Bull. Chem. Soc. Jpn. 79 (2006) 1665–1680. doi:10.1246/bcsj.79.1665.

[20] K. Fumino, A. Wulf, R. Ludwig, The potential role of hydrogen bonding in aprotic and protic ionic liquids, Phys. Chem. Chem. Phys. 11 (2009) 8790. doi:10.1039/b905634c.

[21] R. Hayes, S. Imberti, G.G. Warr, R. Atkin, How Water Dissolves in Protic Ionic Liquids, Angew. Chemie Int. Ed. 51 (2012) 7468–71. doi:10.1002/anie.201201973.

[22] H. Doi, X. Song, B. Minofar, R. Kanzaki, T. Takamuku, Y. Umebayashi, A new proton conductive liquid with no ions: Pseudo-protic ionic liquids, Chem. - A Eur. J. 19 (2013) 11522–11526. doi:10.1002/chem.201302228.

[23] K. Fumino, V. Fossog, P. Stange, K. Wittler, W. Polet, R. Hempelmann, R. Ludwig, Ion Pairing in Protic Ionic Liquids Probed by Far-Infrared Spectroscopy: Effects of Solvent Polarity and Temperature, ChemPhysChem. 15 (2014) 2604–2609. doi:10.1002/cphc.201402205.

[24] H. Watanabe, T. Umecky, N. Arai, A. Nazet, T. Takamuku, K.R. Harris, Y. Kameda, R. Buchner, Y. Umebayashi, Possible Proton Conduction Mechanism in Pseudo-Protic Ionic Liquids: A Concept of Specific Proton Conduction, J. Phys. Chem. B. 123 (2019) 6244–6252. doi:10.1021/acs.jpcb.9b03185.

[25] A.T. Nasrabadi, L.D. Gelb, Structural and Transport Properties of Tertiary Ammonium Triflate Ionic Liquids: A Molecular Dynamics Study, J. Phys. Chem. B. 121 (2017) 1908–1921. doi:10.1021/acs.jpcb.6b12418.

[26] J. Ingenmey, S. Gehrke, B. Kirchner, How to Harvest Grotthuss Diffusion in Protic Ionic Liquid Electrolyte Systems, ChemSusChem. 11 (2018) 1900–1910. doi:10.1002/cssc.201800436.

[27] K. Fumino, A. Wulf, R. Ludwig, Hydrogen Bonding in Protic Ionic Liquids: Reminiscent of Water, Angew. Chemie Int. Ed. 48 (2009) 3184–3186. doi:10.1002/anie.200806224.

[28] S. Menne, J. Pires, M. Anouti, A. Balducci, Protic ionic liquids as electrolytes for lithium-ion batteries, Electrochem. Commun. 31 (2013) 39–41. doi:10.1016/j.elecom.2013.02.026.

[29] V.I. Pârvulescu, C. Hardacre, Catalysis in Ionic Liquids, Chem. Rev. 107 (2007) 2615–2665. doi:10.1021/cr050948h.

[30] A. Mariani, R. Caminiti, F. Ramondo, G. Salvitti, F. Mocci, L. Gontrani, Inhomogeneity in Ethylammonium Nitrate–Acetonitrile Binary Mixtures: The Highest "Low q Excess" Reported to Date, J. Phys. Chem. Lett. 8 (2017) 3512–3522. doi:10.1021/acs.jpclett.7b01244.

[31] A. Mariani, R. Caminiti, L. Gontrani, Water and hexane in an ionic liquid: computational evidence of association under high pressure, Phys. Chem. Chem. Phys. 19 (2017) 8661–8666. doi:10.1039/C6CP08450H.

[32] O. Russina, M. Macchiagodena, B. Kirchner, A. Mariani, B. Aoun, M. Russina, R. Caminiti, A. Triolo, Association in ethylammonium nitrate–dimethyl sulfoxide mixtures: First structural and dynamical evidences, J. Non. Cryst. Solids. 407 (2015) 333–338. doi:10.1016/j.jnoncrysol.2014.08.051.

[33] A. Mariani, O. Russina, R. Caminiti, A. Triolo, Structural organization in a methanol:ethylammonium nitrate (1:4) mixture: A joint X-ray/Neutron diffraction and computational study, J. Mol. Liq. 212 (2015) 947–956. doi:10.1016/j.molliq.2015.10.054.

[34] A. Mariani, R. Dattani, R. Caminiti, L. Gontrani, Nanoscale Density Fluctuations in Ionic Liquid Binary Mixtures with Nonamphiphilic Compounds: First Experimental Evidence, J. Phys. Chem. B. 120 (2016) 10540–10546. doi:10.1021/acs.jpcb.6b07295.

[35] O. Russina, A. Mariani, R. Caminiti, A. Triolo, Structure of a Binary Mixture of Ethylammonium Nitrate and Methanol, J. Solution Chem. 44 (2015) 669–685. doi:10.1007/s10953-015-0311-7.

[36] C.A. Angell, N. Byrne, J.-P. Belieres, Parallel Developments in Aprotic and Protic Ionic Liquids: Physical Chemistry and Applications, Acc. Chem. Res. 40 (2007) 1228–1236. doi:10.1021/ar7001842.

[37] M. Martinez, Y. Molmeret, L. Cointeaux, C. Iojoiu, J.C. Leprêtre, N. El Kissi, P. Judeinstein, J.Y. Sanchez, Proton-conducting ionic liquid-based Proton Exchange Membrane Fuel Cell membranes: The key role of ionomer-ionic liquid interaction, J. Power Sources. 195 (2010) 5829–5839. doi:10.1016/j.jpowsour.2010.01.036.

[38] P. Attri, R. Bhatia, J. Gaur, B. Arora, A. Gupta, N. Kumar, E.H. Choi, Triethylammonium acetate ionic liquid assisted one-pot synthesis of dihydropyrimidinones and evaluation of their antioxidant and antibacterial activities, Arab. J. Chem. 10 (2017) 206–214. doi:10.1016/j.arabjc.2014.05.007.

[39] J. Stoimenovski, E.I. Izgorodina, D.R. MacFarlane, Ionicity and proton transfer in protic ionic liquids, Phys. Chem. Chem.

Phys. 12 (2010) 10341. doi:10.1039/c0cp00239a.
[40] Y. Lv, Y. Guo, X. Luo, H. Li, Infrared spectroscopic study on chemical and phase equilibrium in triethylammonium acetate, Sci. China Chem. 55 (2012) 1688–1694. doi:10.1007/s11426-012-4634-6.
[41] P. Berton, S.P. Kelley, H. Wang, R.D. Rogers, Elucidating the triethylammonium acetate system: Is it molecular or is it ionic?, J. Mol. Liq. 269 (2018) 126–131. doi:10.1016/j.molliq.2018.08.006.
[42] E. Bodo, Structural Features of Triethylammonium Acetate through Molecular Dynamics, Molecules. 25 (2020) 1432. doi:10.3390/molecules25061432.
[43] M. Shen, Y. Zhang, K. Chen, S. Che, J. Yao, H. Li, Ionicity of Protic Ionic Liquid: Quantitative Measurement by Spectroscopic Methods, J. Phys. Chem. B. 121 (2017) 1372–1376. doi:10.1021/acs.jpcb.6b11624.
[44] S.K. Mann, S.P. Brown, D.R. MacFarlane, Structure Effects on the Ionicity of Protic Ionic Liquids, ChemPhysChem. 21 (2020) 1444–1454. doi:10.1002/cphc.202000242.
[45] A.T. Nasrabadi, L.D. Gelb, How Proton Transfer Equilibria Influence Ionic Liquid Properties: Molecular Simulations of Alkylammonium Acetates, J. Phys. Chem. B. 122 (2018) 5961–5971. doi:10.1021/acs.jpcb.8b01631.
[46] D.R. MacFarlane, M. Forsyth, E.I. Izgorodina, A.P. Abbott, G. Annat, K. Fraser, On the concept of ionicity in ionic liquids, Phys. Chem. Chem. Phys. 11 (2009) 4962. doi:10.1039/b900201d.
[47] O. Hollóczki, F. Malberg, T. Welton, B. Kirchner, On the origin of ionicity in ionic liquids. Ion pairing versus charge transfer, Phys. Chem. Chem. Phys. 16 (2014) 16880–16890. doi:10.1039/C4CP01177E.
[48] B. Kirchner, F. Malberg, D.S. Firaha, O. Hollóczki, Ion pairing in ionic liquids, J. Phys. Condens. Matter. 27 (2015) 463002. doi:10.1088/0953-8984/27/46/463002.
[49] T.I. Morrow, E.J. Maginn, Molecular Dynamics Study of the Ionic Liquid 1-n-Butyl-3-methylimidazolium Hexafluorophosphate, J. Phys. Chem. B. 106 (2002) 12807–12813. doi:10.1021/jp0267003.
[50] F. Philippi, D. Rauber, M. Springborg, R. Hempelmann, Density Functional Theory Descriptors for Ionic Liquids and the Charge-Transfer Interpretation of the Haven Ratio, J. Phys. Chem. A. 123 (2019) 851–861. doi:10.1021/acs.jpca.8b10827.
[51] T. Cremer, C. Kolbeck, K.R.J. Lovelock, N. Paape, R. Wölfel, P.S. Schulz, P. Wasserscheid, H. Weber, J. Thar, B. Kirchner, F. Maier, H.-P. Steinrück, Towards a Molecular Understanding of Cation-Anion Interactions-Probing the Electronic Structure of Imidazolium Ionic Liquids by NMR Spectroscopy, X-ray Photoelectron Spectroscopy and Theoretical Calculations, Chem. - A Eur. J. 16 (2010) 9018–9033. doi:10.1002/chem.201001032.
[52] P. Stange, K. Fumino, R. Ludwig, Ion Speciation of Protic Ionic Liquids in Water: Transition from Contact to Solvent-Separated Ion Pairs, Angew. Chemie Int. Ed. 52 (2013) 2990–2994. doi:10.1002/anie.201209609.
[53] K. Fumino, R. Ludwig, Analyzing the interaction energies between cation and anion in ionic liquids: The subtle balance between Coulomb forces and hydrogen bonding, J. Mol. Liq. 192 (2014) 94–102. doi:10.1016/j.molliq.2013.07.009.
[54] K. Fumino, A.-M. Bonsa, B. Golub, D. Paschek, R. Ludwig, Non-Ideal Mixing Behaviour of Hydrogen Bonding in Mixtures of Protic Ionic Liquids, ChemPhysChem. 16 (2015) 299–304. doi:10.1002/cphc.201402760.
[55] S.K. Davidowski, F. Thompson, W. Huang, M. Hasani, S.A. Amin, C.A. Angell, J.L. Yarger, NMR Characterization of Ionicity and Transport Properties for a Series of Diethylmethylamine Based Protic Ionic Liquids, J. Phys. Chem. B. 120 (2016) 4279–4285. doi:10.1021/acs.jpcb.6b01203.
[56] M. Hasani, S.A. Amin, J.L. Yarger, S.K. Davidowski, C.A. Angell, Proton Transfer and Ionicity: An 15 N NMR Study of Pyridine Base Protonation, J. Phys. Chem. B. 123 (2019) 1815–1821. doi:10.1021/acs.jpcb.8b10632.
[57] R. KANZAKI, K. UCHIDA, X. SONG, Y. UMEBAYASHI, S. ISHIGURO, Acidity and Basicity of Aqueous Mixtures of a Protic Ionic Liquid, Ethylammonium Nitrate, Anal. Sci. 24 (2008) 1347–1349. doi:10.2116/analsci.24.1347.
[58] R. Kanzaki, H. Doi, X. Song, S. Hara, S. Ishiguro, Y. Umebayashi, Acid–Base Property of N -Methylimidazolium-Based Protic Ionic Liquids Depending on Anion, J. Phys. Chem. B. 116 (2012) 14146–14152. doi:10.1021/jp308477p.
[59] X. SONG, R. KANZAKI, S. ISHIGURO, Y. UMEBAYASHI, Physicochemical and Acid-base Properties of a Series of 2-Hydroxyethylammonium-based Protic Ionic Liquids, Anal. Sci. 28 (2012) 469–474. doi:10.2116/analsci.28.469.
[60] R. Kanzaki, X. Song, Y. Umebayashi, S. Ishiguro, Thermodynamic Study of the Solvation States of Acid and Base in a Protic Ionic Liquid, Ethylammonium Nitrate, and Its Aqueous Mixtures, Chem. Lett. 39 (2010) 578–579. doi:10.1246/cl.2010.578.
[61] K. Hashimoto, K. Fujii, M. Shibayama, Acid–base property of protic ionic liquid, 1-alkylimidazolium bis(trifluoromethanesulfonyl)amide studied by potentiometric titration, J. Mol. Liq. 188 (2013) 143–147. doi:10.1016/j.molliq.2013.08.023.
[62] J. Ingenmey, M. von Domaros, E. Perlt, S.P. Verevkin, B. Kirchner, Thermodynamics and proton activities of protic ionic liquids with quantum cluster equilibrium theory, J. Chem. Phys. 148 (2018) 193822. doi:10.1063/1.5010791.
[63] C. Schreiner, S. Zugmann, R. Hartl, H.J. Gores, Fractional walden rule for ionic liquids: Examples from recent measurements and a critique of the so-called ideal KCl line for the walden plot, J. Chem. Eng. Data. 55 (2010) 1784–1788. doi:10.1021/je900878j.
[64] M. Yoshizawa, W. Xu, C.A. Angell, Ionic Liquids by Proton Transfer: Vapor Pressure, Conductivity, and the Relevance of Δp K a from Aqueous Solutions, J. Am. Chem. Soc. 125 (2003) 15411–15419. doi:10.1021/ja035783d.
[65] K.R. Harris, On the Use of the Angell–Walden Equation To Determine the "Ionicity" of Molten Salts and Ionic Liquids, J. Phys. Chem. B. 123 (2019) 7014–7023. doi:10.1021/acs.jpcb.9b04443.
[66] J.E. Tanner, Use of the Stimulated Echo in NMR Diffusion Studies, J. Chem. Phys. 52 (1970) 2523–2526.

doi:10.1063/1.1673336.
[67] D.H. Wu, A.D. Chen, C.S. Johnson, An Improved Diffusion-Ordered Spectroscopy Experiment Incorporating Bipolar-Gradient Pulses, J. Magn. Reson. Ser. A. 115 (1995) 260–264. doi:10.1006/jmra.1995.1176.
[68] S.H. Chung, R. Lopato, S.G. Greenbaum, H. Shirota, E.W. Castner, J.F. Wishart, Nuclear magnetic resonance study of the dynamics of imidazolium ionic liquids with -CH2Si(CH3)3 vs -CH 2C(CH3)3 substituents, J. Phys. Chem. B. 111 (2007) 4885–4893. doi:10.1021/jp071755w.
[69] K. Hayamizu, Y. Aihara, H. Nakagawa, T. Nukuda, W.S. Price, Ionic Conduction and Ion Diffusion in Binary Room-Temperature Ionic Liquids Composed of [emim][BF 4] and LiBF 4, J. Phys. Chem. B. 108 (2004) 19527–19532. doi:10.1021/jp0476601.
[70] C.J.F. Solano, S. Jeremias, E. Paillard, D. Beljonne, R. Lazzaroni, A joint theoretical/experimental study of the structure, dynamics, and Li+ transport in bis([tri]fluoro[methane]sulfonyl)imide [T]FSI-based ionic liquids, J. Chem. Phys. 139 (2013). doi:10.1063/1.4813413.
[71] A. Mariani, M. Bonomo, B. Wu, B. Centrella, D. Dini, E.W. Castner, L. Gontrani, Intriguing transport dynamics of ethylammonium nitrate–acetonitrile binary mixtures arising from nano-inhomogeneity, Phys. Chem. Chem. Phys. 19 (2017) 27212–27220. doi:10.1039/C7CP04592A.
[72] M. Campetella, A. Mariani, C. Sadun, B. Wu, E.W. Castner, L. Gontrani, Structure and dynamics of propylammonium nitrate-acetonitrile mixtures: An intricate multi-scale system probed with experimental and theoretical techniques, J. Chem. Phys. 148 (2018) 134507. doi:10.1063/1.5021868.
[73] G. Annat, D.R. MacFarlane, M. Forsyth, Transport properties in ionic liquids and ionic liquid mixtures: The challenges of NMR pulsed field gradient diffusion measurements, J. Phys. Chem. B. 111 (2007) 9018–9024. doi:10.1021/jp072737h.
[74] J.L. Lebga-Nebane, S.E. Rock, J. Franclemont, D. Roy, S. Krishnan, Thermophysical Properties and Proton Transport Mechanisms of Trialkylammonium and 1-Alkyl-1 H -imidazol-3-ium Protic Ionic Liquids, Ind. Eng. Chem. Res. 51 (2012) 14084–14098. doi:10.1021/ie301687c.
[75] D.M. Jollie, P.G. Harrison, An in situ IR study of the thermal decomposition of trifluoroacetic acid, J. Chem. Soc. Perkin Trans. 2. (1997) 1571–1575. doi:10.1039/a608233e.
[76] T. Burankova, R. Hempelmann, V. Fossog, J. Ollivier, T. Seydel, J.F. Embs, Proton Diffusivity in the Protic Ionic Liquid Triethylammonium Triflate Probed by Quasielastic Neutron Scattering, J. Phys. Chem. B. 119 (2015) 10643–10651. doi:10.1021/acs.jpcb.5b04000.
[77] M.S. Miran, H. Kinoshita, T. Yasuda, M.A.B.H. Susan, M. Watanabe, Physicochemical properties determined by ΔpKa for protic ionic liquids based on an organic super-strong base with various Brønsted acids, Phys. Chem. Chem. Phys. 14 (2012) 5178. doi:10.1039/c2cp00007e.
[78] P.K. Chhotaray, R.L. Gardas, Thermophysical properties of ammonium and hydroxylammonium protic ionic liquids, J. Chem. Thermodyn. 72 (2014) 117–124. doi:10.1016/j.jct.2014.01.004.
[79] L.E. Shmukler, M.S. Gruzdev, N.O. Kudryakova, Y.A. Fadeeva, A.M. Kolker, L.P. Safonova, Thermal behavior and electrochemistry of protic ionic liquids based on triethylamine with different acids, RSC Adv. 6 (2016) 109664–109671. doi:10.1039/C6RA21360J.
[80] L.E. Shmukler, M.S. Gruzdev, N.O. Kudryakova, Y.A. Fadeeva, A.M. Kolker, L.P. Safonova, Triethylammonium-based protic ionic liquids with sulfonic acids: Phase behavior and electrochemistry, J. Mol. Liq. 266 (2018) 139–146. doi:10.1016/j.molliq.2018.05.059.
[81] G.L. Burrell, I.M. Burgar, F. Separovic, N.F. Dunlop, Preparation of protic ionic liquids with minimal water content and 15N NMR study of proton transfer, Phys. Chem. Chem. Phys. 12 (2010) 1571. doi:10.1039/b921432a.
[82] C. Iojoiu, M. Martinez, M. Hanna, Y. Molmeret, L. Cointeaux, J.-C. Leprêtre, N. El Kissi, J. Guindet, P. Judeinstein, J.-Y. Sanchez, PILs-based Nafion membranes: a route to high-temperature PEFMCs dedicated to electric and hybrid vehicles, Polym. Adv. Technol. 19 (2008) 1406–1414. doi:10.1002/pat.1219.
[83] H. Nakamoto, M. Watanabe, Brønsted acid–base ionic liquids for fuel cell electrolytes, Chem. Commun. (2007) 2539–2541. doi:10.1039/B618953A.
[84] C. Iojoiu, P. Judeinstein, J.Y. Sanchez, Ion transport in CLIP: Investigation through conductivity and NMR measurements, Electrochim. Acta. 53 (2007) 1395–1403. doi:10.1016/j.electacta.2007.04.065.
[85] Y. Kohno, H. Ohno, Ionic liquid/water mixtures: from hostility to conciliation, Chem. Commun. 48 (2012) 7119. doi:10.1039/c2cc31638b.
[86] C. Iojoiu, M. Hana, Y. Molmeret, M. Martinez, L. Cointeaux, N. El Kissi, J. Teles, J.C. Leprêtre, P. Judeinstein, J.Y. Sanchez, Ionic liquids and their hosting by polymers for HT-PEMFC Membranes, Fuel Cells. 10 (2010) 778–789. doi:10.1002/fuce.201000026.
[87] J.A. Bautista-Martinez, L. Tang, J.-P. Belieres, R. Zeller, C.A. Angell, C. Friesen, Hydrogen Redox in Protic Ionic Liquids and a Direct Measurement of Proton Thermodynamics, J. Phys. Chem. C. 113 (2009) 12586–12593. doi:10.1021/jp902762c.
[88] H. Mauser, A. Albert und E. P. Serjeant: Ionization Constants of Acids and Bases. 1. Auflage. Methuen & Co., London, John Wiley Sons, New York 1962. 179 Seiten 8° und 9 Abbildungen im Text. Preis: 21/-s, Berichte Der Bunsengesellschaft Für Phys. Chemie. 66 (1962) 882–882. doi:10.1002/BBPC.19620661025.
[89] J.A. Riddick, W.B. Bunger, T.K. Sakano, Organic Solvents: Physical Properties and Methods of Purification (Techniques of

Chemistry, Vol. II) John A. Riddick (Baton Rouge, La.) and William B. Bunger (Indiana State University, Terre Haute, Ind.) Wiley-Interscience, New York/London/Sydney/Toronto, J. Chromatogr. Sci. 12 (1974) 38A-38A. doi:10.1093/chromsci/12.2.38A-b.

[90] J.B. Milne, T.J. Parker, Dissociation constant of aqueous trifluoroacetic acid by cryoscopy and conductivity, J. Solution Chem. 10 (1981) 479–487. doi:10.1007/BF00652082.

[91] A. Trummal, L. Lipping, I. Kaljurand, I.A. Koppel, I. Leito, Acidity of Strong Acids in Water and Dimethyl Sulfoxide, J. Phys. Chem. A. 120 (2016) 3663–3669. doi:10.1021/acs.jpca.6b02253.

[92] A.K. Chandra, A. Goursot, Calculation of proton affinities using density functional procedures: A critical study, J. Phys. Chem. 100 (1996) 11596–11599. doi:10.1021/jp9603750.

[93] P. Bonhôte, A.-P. Dias, M. Armand, N. Papageorgiou, K. Kalyanasundaram, M. Grätzel, Hydrophobic, Highly Conductive Ambient-Temperature Molten Salts, Inorg. Chem. 37 (1998) 166–166. doi:10.1021/ic971286k.

[94] A.P. Abbott, Model for the Conductivity of Ionic Liquids Based on an Infinite Dilution of Holes, ChemPhysChem. 6 (2005) 2502–2505. doi:10.1002/cphc.200500283.

[95] Y.H. Zhao, M.H. Abraham, A.M. Zissimos, Fast Calculation of van der Waals Volume as a Sum of Atomic and Bond Contributions and Its Application to Drug Compounds, J. Org. Chem. 68 (2003) 7368–7373. doi:10.1021/jo034808o.

[96] K. Fumino, S. Reimann, R. Ludwig, Probing molecular interaction in ionic liquids by low frequency spectroscopy: Coulomb energy, hydrogen bonding and dispersion forces, Phys. Chem. Chem. Phys. 16 (2014) 21903–21929. doi:10.1039/C4CP01476F.

[97] K. Fumino, V. Fossog, P. Stange, D. Paschek, R. Hempelmann, R. Ludwig, Controlling the Subtle Energy Balance in Protic Ionic Liquids: Dispersion Forces Compete with Hydrogen Bonds, Angew. Chemie Int. Ed. 54 (2015) 2792–2795. doi:10.1002/anie.201411509.

[98] K. Fumino, E. Reichert, K. Wittler, R. Hempelmann, R. Ludwig, Low Frequency Vibrational Modes of Protic Molten Salts and Ionic Liquids: Detecting and Quantifying Hydrogen Bonds, Angew. Chemie Int. Ed. 51 (2012) 6236–6240. doi:10.1002/anie.201200508.

[99] A. Mariani, M. Campetella, C. Fasolato, M. Daniele, F. Capitani, L. Bencivenni, P. Postorino, S. Lupi, R. Caminiti, L. Gontrani, M. Campetella, C. Fasolato, F. Capitani, P. Postorino, C. Fasolato, M. Daniele, S. Lupi, R. Caminiti, F. Capitani, L. Bencivenni, P. Postorino, S. Lupi, R. Caminiti, L. Gontrani, A joint experimental and computational study on ethylammonium nitrate-ethylene glycol 1:1 mixture. Structural, kinetic, dynamic and spectroscopic properties, J. Mol. Liq. 226 (2017) 2–8. doi:10.1016/j.molliq.2016.08.043.

[100] V.H. Paschoal, L.F.O. Faria, M.C.C. Ribeiro, Vibrational Spectroscopy of Ionic Liquids, Chem. Rev. 117 (2017) 7053–7112. doi:10.1021/acs.chemrev.6b00461.

[101] V.N. Emel'yanenko, G. Boeck, S.P. Verevkin, R. Ludwig, Volatile times for the very first ionic liquid: Understanding the vapor pressures and enthalpies of vaporization of ethylammonium nitrate, Chem. - A Eur. J. 20 (2014) 11640–11645. doi:10.1002/chem.201403508.

[102] A.B. Patil, B.M. Bhanage, Assessing ionicity of protic ionic liquids by far IR spectroscopy, J. Mol. Liq. 252 (2018) 180–183. doi:10.1016/j.molliq.2017.12.131.

[103] G. Gamer, H. Wolff, Raman and infrared spectra of gaseous secondary aliphatic amines [(CH32NH, (CH3)2ND, (C2H5)2NH and C2H5NHCH3], Spectrochim. Acta Part A Mol. Spectrosc. 29 (1973) 129–137. doi:10.1016/0584-8539(73)80015-7.

[104] Triethylamine FTIR spectrum (https://webbook.nist.gov/cgi/cbook.cgi?ID=C121448&Type=IR-SPEC&Index=1#IR-SPEC), Https://Webbook.Nist.Gov/Cgi/Cbook.Cgi?ID=C121448&Type=IR-SPEC&Index=1#IR-SPEC. (n.d.).

[105] C.P. Rosenau, B.J. Jelier, A.D. Gossert, A. Togni, Exposing the Origins of Irreproducibility in Fluorine NMR Spectroscopy, Angew. Chemie - Int. Ed. 57 (2018) 9528–9533. doi:10.1002/anie.201802620.

[106] T. Takamuku, Y. Kyoshoin, H. Noguchi, S. Kusano, T. Yamaguchi, Liquid Structure of Acetic Acid−Water and Trifluoroacetic Acid−Water Mixtures Studied by Large-Angle X-ray Scattering and NMR, J. Phys. Chem. B. 111 (2007) 9270–9280. doi:10.1021/jp0724976.

[107] A. Mariani, R. Caminiti, M. Campetella, L. Gontrani, Pressure-induced mesoscopic disorder in protic ionic liquids: first computational study, Phys. Chem. Chem. Phys. 18 (2016) 2297–2302. doi:10.1039/C5CP06800B.

[108] R. Hayes, S. Imberti, G.G. Warr, R. Atkin, Amphiphilicity determines nanostructure in protic ionic liquids, Phys. Chem. Chem. Phys. 13 (2011) 3237–3247. doi:10.1039/C0CP01137A.

[109] R. Atkin, G.G. Warr, The Smallest Amphiphiles: Nanostructure in Protic Room-Temperature Ionic Liquids with Short Alkyl Groups, J. Phys. Chem. B. 112 (2008) 4164–6. doi:10.1021/jp801190u.

[110] D. Pontoni, J. Haddad, M. Di Michiel, M. Deutsch, Self-segregated nanostructure in room temperature ionic liquids, Soft Matter. 13 (2017) 6947–6955. doi:10.1039/C7SM01464C.

[111] M. Brehm, H. Weber, M. Thomas, O. Hollóczki, B. Kirchner, Domain Analysis in Nanostructured Liquids: A Post-Molecular Dynamics Study at the Example of Ionic Liquids, ChemPhysChem. 16 (2015) 3271–3277. doi:10.1002/cphc.201500471.

[112] T.L. Greaves, D.F. Kennedy, N. Kirby, C.J. Drummond, Nanostructure changes in protic ionic liquids (PILs) through adding solutes and mixing PILs, Phys. Chem. Chem. Phys. 13 (2011) 13501. doi:10.1039/c1cp20496c.

[113] J.N.A. Canongia Lopes, A.A.H. Pádua, Nanostructural Organization in Ionic Liquids, J. Phys. Chem. B. 110 (2006) 3330–3335. doi:10.1021/jp056006y.

[114] O. Suárez-Iglesias, I. Medina, C. Pizarro, J.L. Bueno, On predicting self-diffusion coefficients from viscosity in gases and liquids, Chem. Eng. Sci. 62 (2007) 6499–6515. doi:10.1016/j.ces.2007.07.004.

[115] W. Hayduk, S.C. Cheng, Review of relation between diffusivity and solvent viscosity in dilute liquid solutions, Chem. Eng. Sci. 26 (1971) 635–646. doi:10.1016/0009-2509(71)86007-4.

[116] T. Köddermann, R. Ludwig, D. Paschek, On the validity of Stokes-Einstein and Stokes-Einstein-Debye relations in ionic liquids and ionic-liquid mixtures, ChemPhysChem. 9 (2008) 1851–1858. doi:10.1002/cphc.200800102.

[117] M. Kar, N. V. Plechkova, K.R. Seddon, J.M. Pringle, D.R. MacFarlane, Ionic Liquids – Further Progress on the Fundamental Issues, Aust. J. Chem. 72 (2019) 3. doi:10.1071/CH18541.

[118] M.J. Frisch, G.W. Trucks, H.B. Schlegel, G.E. Scuseria, M.A. Robb, J.R. Cheeseman, G. Scalmani, V. Barone, G.A. Petersson, H. Nakatsuji, X. Li, M. Caricato, A. Marenich, J. Bloino, B.G. Janesko, R. Gomperts, B. Mennucci, H.P. Hratchian, J. V. Ort, D.J. Fox, Gaussian 09, Revision D.01, (2009).

[119] M.D. Hanwell, D.E. Curtis, D.C. Lonie, T. Vandermeersch, E. Zurek, G.R. Hutchison, Avogadro: an advanced semantic chemical editor, visualization, and analysis platform, J. Cheminform. 4 (2012) 17. doi:10.1186/1758-2946-4-17.

[120] M.H. Jamróz, Vibrational Energy Distribution Analysis (VEDA): Scopes and limitations, Spectrochim. Acta Part A Mol. Biomol. Spectrosc. 114 (2013) 220–230. doi:10.1016/j.saa.2013.05.096.

Author Contributions

All authors have given approval to the final version of the manuscript. AM and MB contributed to the same extent to the manuscript by conceptualization, interpretation of the results, and writing the manuscript. XG synthesized the PILs and collected DSC, TGA, conductivity, and viscosity data. AN supervised the FIR experiments. BC and NB performed 1H and 13C NMR measurements. RB and AB supervised the NMR experiments and performed 19F and PGSE NMR measurements. LG and SP edited the drafts and supervised the project.

Highlights

- The ambiguity between proton transfer and ionicity is resolved by the introduction of Reduced Ionicity
- The current literature regarding ioniciy in protic ionic liquids is critically revised
- The role of pKa and proton affinity in protic ionic liquids is elucidated

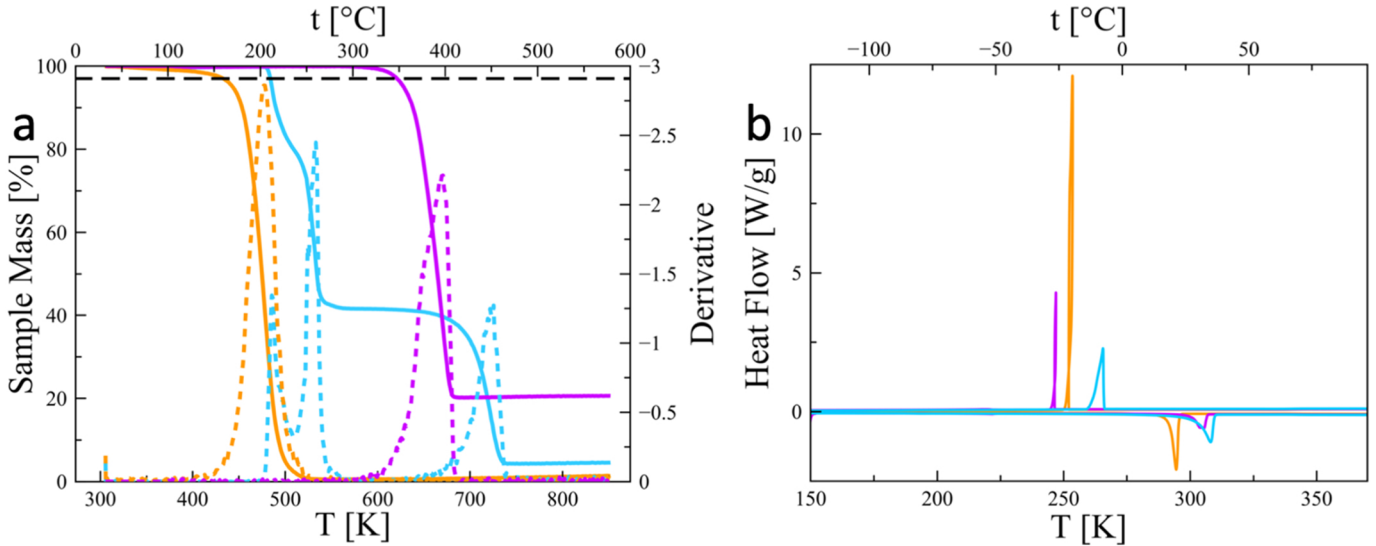
a
t [°C]
0
100
200
300
400
500
600
Sample Mass [%]
100
80
60
40
20
0
Derivative
−3
−2.5
−2
−1.5
−1
−0.5
0
300
400
500
600
700
800
T [K]
b
t [°C]
−100
−50
0
50
Heat Flow [W/g]
10
5
0
150
200
250
300
350
T [K]

Figure 1

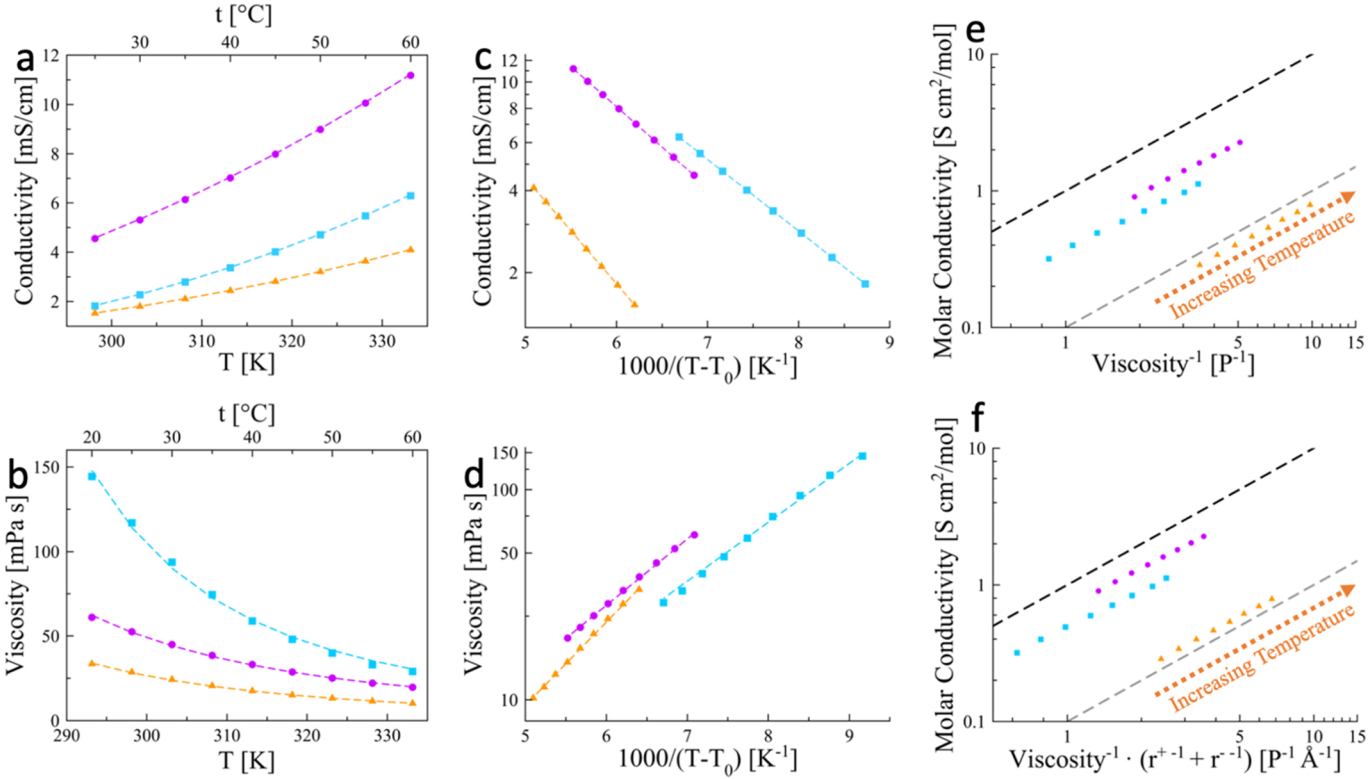
a
t [°C]
30
40
50
60
Conductivity [mS/cm]
T [K]
b
Viscosity [mPa s]
c
1000/(T-T0) [K-1]
d
e
Molar Conductivity [S cm2/mol]
Viscosity-1 [P-1]
Increasing Temperature
f
Viscosity-1 · (r+ -1 + r- -1) [P-1 Å-1]

Figure 2

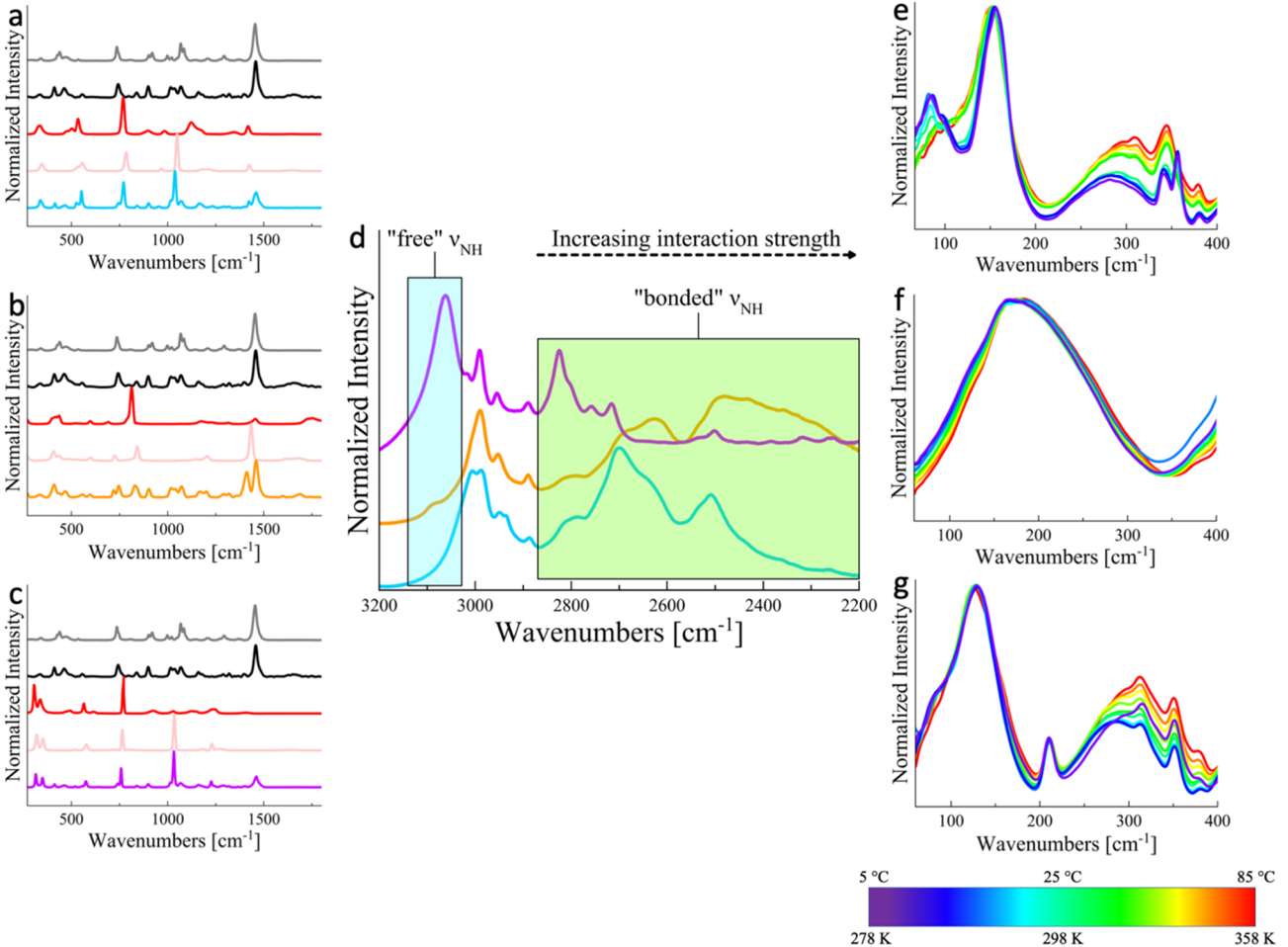
a
Normalized Intensity
500
1000
1500
Wavenumbers [cm-1]
b
Normalized Intensity
500
1000
1500
Wavenumbers [cm-1]
c
Normalized Intensity
500
1000
1500
Wavenumbers [cm-1]
d
"free" νNH
Increasing interaction strength
"bonded" νNH
Normalized Intensity
3200
3000
2800
2600
2400
2200
Wavenumbers [cm-1]
e
Normalized Intensity
100
200
300
400
Wavenumbers [cm-1]
f
Normalized Intensity
100
200
300
400
Wavenumbers [cm-1]
g
Normalized Intensity
100
200
300
400
Wavenumbers [cm-1]
5 °C
25 °C
85 °C
278 K
298 K
358 K

Figure 3

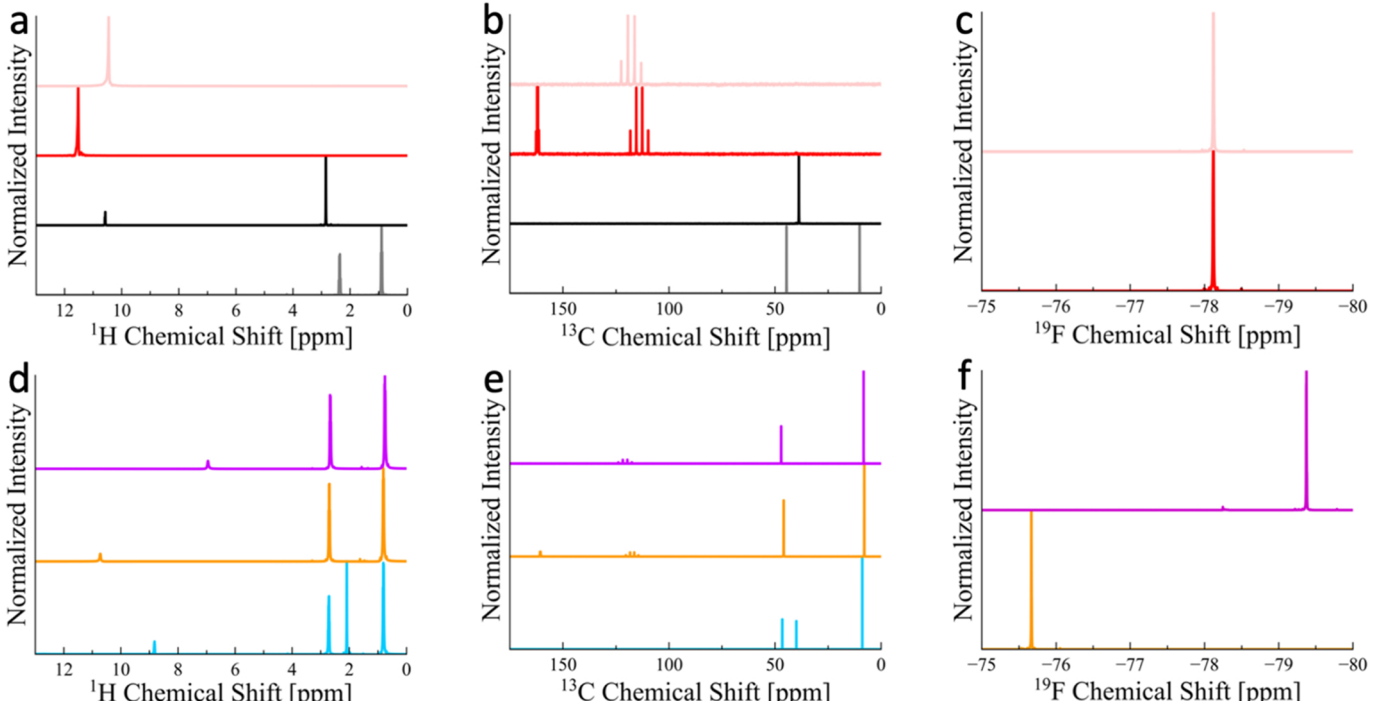
a
Normalized Intensity
12
10
8
6
4
2
0
^{1}H Chemical Shift [ppm]
b
Normalized Intensity
150
100
50
0
^{13}C Chemical Shift [ppm]
c
Normalized Intensity
−75
−76
−77
−78
−79
−80
^{19}F Chemical Shift [ppm]
d
Normalized Intensity
12
10
8
6
4
2
0
^{1}H Chemical Shift [ppm]
e
Normalized Intensity
150
100
50
0
^{13}C Chemical Shift [ppm]
f
Normalized Intensity
−75
−76
−77
−78
−79
−80
^{19}F Chemical Shift [ppm]

Figure 4

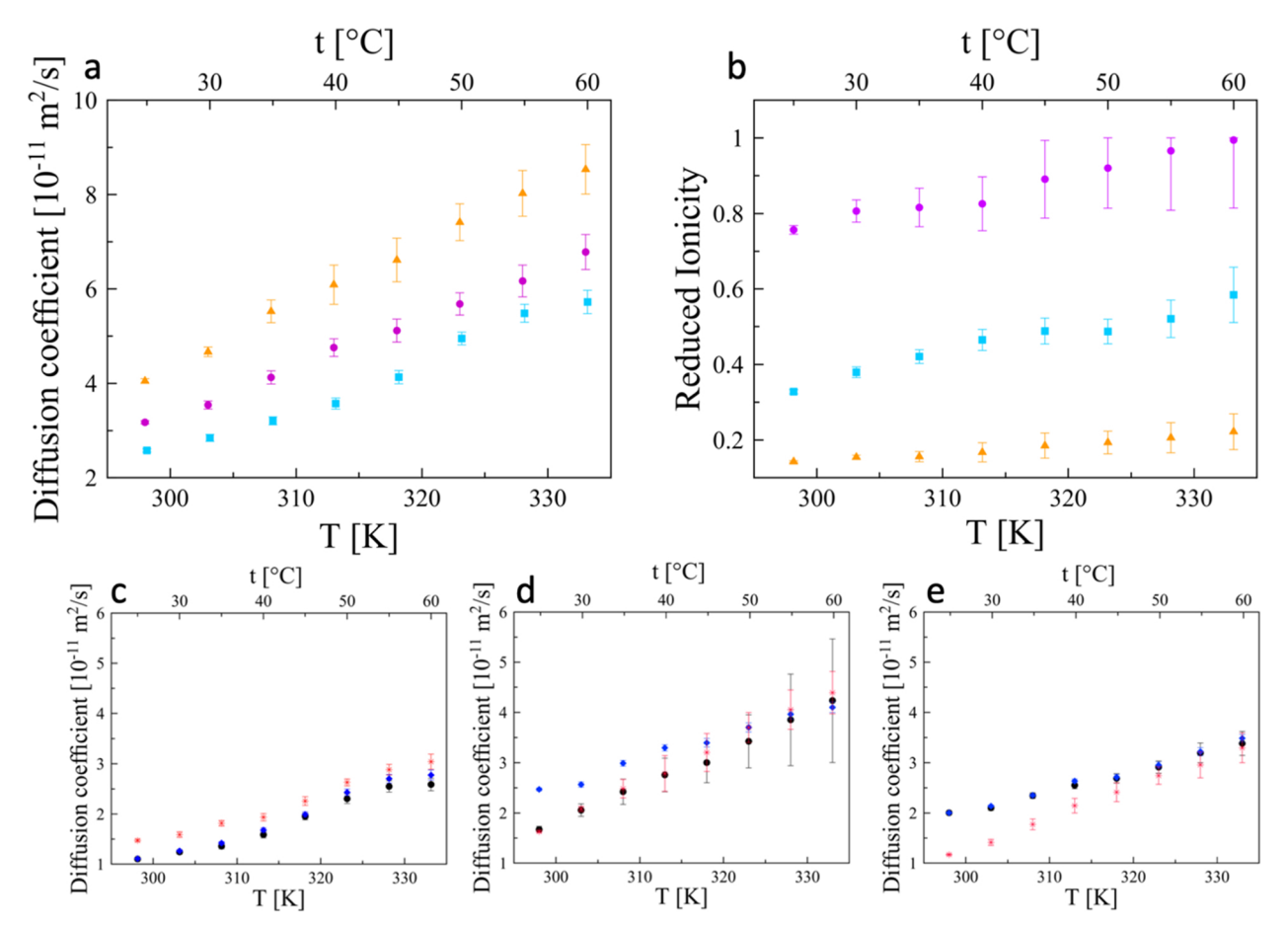
a
t [°C]
30
40
50
60
Diffusion coefficient [10^-11 m^2/s]
10
8
6
4
2
300
310
320
330
T [K]
b
t [°C]
30
40
50
60
Reduced Ionicity
1
0.8
0.6
0.4
0.2
300
310
320
330
T [K]
c
t [°C]
30
40
50
60
Diffusion coefficient [10^-11 m^2/s]
6
5
4
3
2
1
300
310
320
330
T [K]
d
t [°C]
30
40
50
60
Diffusion coefficient [10^-11 m^2/s]
6
5
4
3
2
1
300
310
320
330
T [K]
e
t [°C]
30
40
50
60
Diffusion coefficient [10^-11 m^2/s]
6
5
4
3
2
1
300
310
320
330
T [K]

Figure 5